THE ROLE OF COPPER IONS AND OTHER CATHODIC DEPOLARIZERS IN THE CORROSION OF ALUMINUM IN SEAWATER

By

Samuel W. Smith, Jr.

Ronald M. Latanision

Sea Grant College Program
Massachusetts Institute of Technology
Cambridge, Massachusetts 02139

Internal Report
Grant # NA 79AA-D-00[illegible]
Project #

Table of Contents

Introduction:

Aluminum, with its high strength to weight ratio, corrosion resistance, and moderate cost, is a very attractive metal for use in the marine environment. The major factor limiting aluminum's use is its suseptability to localized corrosion. The cathodic reactions appear to be the rate limiting step for the localized corrosion of aluminum (Dexter 1979A). Any reduction in cathodic rates would therefore be reflected in a reduced corrosion rate. The objective of this research was to give some insight into these cathodic processes as they occur on aluminum in seawater.

Cathodic processes give few, if any, visual clues to their presence. In order to determine their locations a specialized piece of equipment had to be built. This device measures the electric field in the electrolyte just above the specimen's surface during the corrosion process. For this reason the device has been named the Scanning Potential Microprobe (SPM). With the SPM sites of cathodic activity were investigated.

Once the surface electrochemistry was determined the surface morphology was evaluated. A Scanning Auger Microprobe (SAM) (Physical Electronics Industries model 590A) was used to analyse the surface. SAM allows secondary electron images, surface composition, surface distribution, and composition depth profiles be obtained.

Computer chemical speciation models were used to investigate the role of surface films in the corrosion reaction.

Scanning Potential Microprobe

As proposed, a potential scanning device was constructed which can record the potential field just above a corrosion specimen. This piece of equipment was modeled after the Scanning Potential Microprobe (SPM) at the Brookhaven National Labs designed by Mr. Hugh Isaacs (Isaacs, 1974).

The SPM is pictured in Figure 1 with a close up of the stage in Figure 2. The SPM measures small variations in the potential field above a specimen's surface by subtracting the average potential of the corrosion specimen from the potential measured by a micro-electrode moving just above the specimen. Both the average potential measuring electrode and the micro-electrode consist of Saturated Calomel Electrodes. Stepping motors move the microelectrode over the specimen. Potentiometers attached to the motors' shafts allow determination of the micro-electrode's position.

An example of SPM data is found in Figure 3. The noise level is on the order of 0.007mV in amplitude. This corresponds to the noise level expected from the electrometers. In order to achieve this noise level all data lines are fully shielded coaxial cables. In addition, the electrometers are kept separate from all power supplies and the stepping motors. A Faraday cage around the stage was found to have a negligable effect on the noise level. The SPM has a lateral resolution of approximately 0.2mm. Its detection

limit is governed by the strength of the electric field generated by a given feature, rather than the size of the feature. The field must be above noise to be detected.

A block diagram of the SPM is shown in Figure 4. The apparatus consists of a Digital Controller which controls the stepping motor logic, the Translator Panel that interfaces the Digital Controller with the stepping motors, the Power Supply which energizes the stepping motors, the Summer which adds data to position information, the X-Y Plotter which graphs the data, and a Stage which houses the specimen tray, electrodes, and stepping motors. Each component will be discussed in detail below.

The Digital Controller is a TTL logic digital circuit outputting a series of pulses which move the probe in conjunction with the Translator Modules and stepping motors. Its schematic is shown in Figure 5. The circuit is modeled after that used in the Brookhaven National Lab SPM. The output of the Controller consists of four data lines, two for the X (forward and reverse) and two for the Y direction. The Digital Controller moves the probe in a straight line mode or a raster pattern with the operater controlling line width, line spacing, and number of lines scanned. The Controller homes the probe after the raster pattern is completed. Each time a step is to be taken be the probe (it moves in discrete steps rather than continuously) a pulse is output by the Controller on the appropriate data line.

The Translator Modules contain the logic which converts pulses

from the digital controller to the appropriate energizing and de-energizing of motor coils to cause the motor to move one step. Two Superior Electric model STM-103 Translator Modules are used for this purpose. They are capable of driving the stepping motors in either full step (1.8^{o}) or half step (0.9^{o}) mode. The modules have adjustable acceleration and deceleration for starting and stopping the motors smoothly. They have separate internal oscillators and a two windings on mode which allows the torque to be increased about 20%. Basically these units act as electronic distributors for the power to the motors.

The motors are powered by a 24 volt, 10 amp fully regulated power supply. A Superior Electric model MPS-3000 transformer is used. This unit provides enough current to power both stepping motors (Superior Electric SLO-SYN model M062-FC03). It also powers the Translator Modules and the potentiometers which allow determination the probe position. The power supply is connected to the stage via a 12 foot cable consisting of 12 strands of 16 gage wire (for motor power) and two strands of shielded coaxial cable (to record probe position). This panel also houses four 13 ohm, 160 watt resistors. These drop the 24 volt transformer output to the 5.4 volts used by the motors. This is necessary since a 5.4 volt transformer can not supply current quickly enough to energize the motor coils at the rate needed to step the motors smoothly.

The stepping motors are mounted on a heavy cast iron base

(Brown & Sharp, Inc.) to reduce vibration due to the motors (Figure 2). The motors move an X-Y stage constructed from two five inch ball bearing slides (Automation Gauges). The electrodes are held in position in the plastic specimen tray by test tube clamps. The micro-electrode is attached to the X-Y stage and held just above the specimen. The electrode which measures average potential is clamped to a stationary rod 3 to 5cm from the specimen. The specimen is mounted on a microscope slide and placed in the specimen tray. This tray can be leveled by means of three set screws in its base. Commercial purity aluminum sheet of 1mm thickness was used to construct the samples. This was cut into 1cm squares and the back and edges were coated with laquer (Stop-Off) so that an area of $1cm^2$ was exposed to the solution.

The electrode electronics are entirely separate from the motor electronics. This is done to reduce noise. Potential measurements are made via two Fisher Electronics Saturated Calomel Electrodes. The specimen's average potential is measured with a porous plug (model 13-639-52), chosen for its ruggedness. The micro-electrode utilizes a cracked bead electrode (model 13-639-57) to minimize leakage from the microelectrode's capillary. Figure 6 shows the construction of the micro-electrode. A capillary diameter of 0.1mm was strived for. This allows sufficient current for accurate measurement with acceptable spacial resolution. The probe is filled with seawater so that any leakage from the capillary which might occur will have a minimum effect on the reactions ocurring on

the specimen's surface.

The electrode potentials are measured by two battery powered Kiethly model 602 electrometers. The battery powered electerometers have lower noise levels than AC operated models. They also reduce the danger of electric shock while working with seawater. The electrometers are connected with the unity gain output of the electrometer which measures the average potential providing the low input of the micro-electrode's electrometer. In this configuration the electrometers act as a differential amplifier with the low lead of the micro-electrode's electrometer at ground (Figure 7). This output is then feed to the Summer.

The Summer takes the output of the electrometers and adds it to the voltage across the potentiometer which measures the micro-electrode's position in the Y direction. This is accomplished by use of a simple IC circuit as shown in Figure 8. This circuit has a better than 4MEG input impedance and better than 8MEG isolation between inputs. It is powered by a fully regulated +/- 5 volt power supply.

The data is output on an X-Y plotter (MFP model 815M). The voltages from the potentiometers attached to the motor shafts are input to the plotter. Since these voltages vary liniarly with shaft position the pen of the plotter is rastered with the micro-electrode. As the pen is rastered the output of the electrometers is summed with the Y channel. This yields a quasi-three dimensional representation of the potential field above

the specimen's surface (Figure 3). The pen is deflected upward when an anodic field is encountered and downward by cathodic fields.

By superimposing a raster plot with no electrometer signal over the original data plot and coloring the graph a clearer visualization of the potential trends on the surface could be obtained. The areas where the pen deflected upward (anodes) were colored blue and the areas where the pen deflected downward (cathodes) were colored green (Figure 9). If the raster pattern has been properly placed the area of deflection above the line equals the area of deflection below the line. This is required by charge balance. It was not really necessary to have the areas exactly equal since areas of small potential field were of relatively little interest. A comparason of Figures 9 and 3 illustrate the usefullness of this technique.

The SPM data collected does not support the existance of preferential cathodes which are of comparable size and strength to anodic sites (pits). The data does show that some areas of the surface appear to have stronger cathodic activity than others. This data does not rule out the possibility of descrete cathodic sites, since they were probably more closely spaced that the spacial resolution of the SPM. The zone of cathodic potential which should have existed around a pit was not detected by the SPM. This cathodic zone was expected since the solution path resistance would be lowest in this area. This cathodic signal

(excess anions in solution) was probably screened by the cations produced at the anode.

Scanning Auger Microprobe

In Scanning Auger Microscopy (SAM) one bombards the surface of a material with a beam of electrons. As these electrons hit the atoms comprising the surface of the sample, they knock some of the electrons in these atom's inner shells to higher energy states. Since this is not stable, these high energy electrons decay to their inner shells with a release of energy. This energy can either be in the form of an emitted photon or electron. The emitted electrons are called Auger electrons after their discoverer. The SAM measures the energies of these electrons, which are characteristic of the emitting element.

The SAM will allow a lateral resolution of up to 0.1 micron with a sample penetration of about 10 atomic layers (MacDonald, et al, 1976). The electron beam can either be held stationary or rastered over the surface. If the energy range from 0 to 2000eV is scanned the resulting graph shows a positive then negative peak at the appropriate energy for each element present (this is due to the fact that the derivative of the electron current with respect to energy is actually plotted). Since the technique has a different sensitivity for each element (Table 1), the peak height must be divided by the sensitivity of the element if comparasons are to be made between elements on the same plot. By rastering the electron beam at a particular element's energy, a map of elemental distribution can be obtained. Another feature of the SAM is the

ability to sputter away the surface with an Argon ion beam while still making elemental analysis. This allows composition depth profiles to be obtained. The same samples were used for both SAM and SPM analysis.

The initial series of tests were designed to determine the compositional differences between oxide films formed in distilled water, 0.7 molar NaCl, natural seawater, and natural seawater contaminated with copper sulfate. Copper sulfate was used to add copper since as a salt of a major element of seawater it will have an insignificant effect on sulfate concentrations in the test solutions. The samples were prepared by abrading with 600 grit wet-dry sand paper, then holding several hours in a desiccator to allow generation of an air formed oxide film. The samples were then placed in the appropriate solution for 24 hours. Upon removal from the solution the samples were washed in acetone and placed in a desiccator.

The sample held in triply distilled water showed very few impurities (Figure 10) on its surface. The major surface elements were, as expected aluminum and oxygen. The small carbon and chloride peaks were probably due to contamination of the surface during transport from the lab to the SAM facility. This type of contamination is nearly impossible to prevent. Some of the samples did show a small silicon peak. At the levels that were present on the samples the silicon should have had little effect on the results.

A typical SAM spectrum for the samples held in 0.7 molar NaCl solution is shown in Figure 11. The solution consisted of triply distilled water and reagent grade Sodium Chloride. The only difference between the film composition in this solution and that in distilled water was the appearance of a sodium peak and an increase in the chloride peak. This result was hardly unexpected. One sample did, however, show significant iron and copper peaks. This was traced to rinsing the sample in tap water during abrasion. This points out both the care which had be taken in sample preparation and the highly reactive nature of the aluminium surface.

The films formed on an aluminum surface in seawater were very much more complex than those found in the previous two cases. As can be seen in Figure 12, this surface was comprised of sulfur, calcium, nitrogen, sodium, magnesium, aluminum, chlorine, silicon, carbon, and oxygen. A trace amount of copper was difficult to rule out due to interference by the sodium peak, but any significant level appears unlikely. The calcium was possibly present as calcium carbonate which had precipitated on the surface from seawater. The sulfur and nitrogen may be associated with organics present on the surface or they may have been from the evaporation of residual seawater on the surface. The biggest surprise was the magnitude of the magnesium peak. Morse (1979) also reported magnesium association with aluminum surfaces in seawater. Thermodynamically one would not expect magnesium ions to be reduced

onto the surface in the manner of copper and iron ions. The magnesium problem will be discussed in greater detail later.

When the seawater was contaminated with copper ions, the aluminum samples produced SAM spectra typical of Figure 13. This specrum shows all the elements found in the seawater film plus copper. Figures 14 and 15 show a secondary electron scan of a typical surface and the corresponding copper map. This map shows a considerable variation in the copper particle size. There appears to be a considerable fraction present as small dispersed particles. At this time it is not know if the copper is in the metallic state or not. If the copper is adsorbed onto the aluminum surface by a copper reduction-aluminum oxidation exchange reaction one would expect the copper to be in the reduced state.

In order to determine how the films develop in seawater a series of tests were run with samples immersed in seawater for 30 minutes, 11 hours, and 24 hours. Auger spectra and composition verses depth profiles were run for a control sample with an air formed film and the 30 minute and 11 hour samples, the 24 hour sample could not be analysed due to charging (the build up of charge at a site due to non-conduction which deflects the electron beam). The beam energy used would yield a sputtering rate of 100A per minute if the Argon beam were sputtering tantalum, the only element for which good data exist. Exactly what the sputtering rate was in aluminum is not known. The pen moves at the rate of 0.5 inches per minute. In these profiles the line height is not

indicative of concentration. Unfortunately the magnesium levels in these specimens were too low to be measured accurately, this is believed due to use of a distilled water rinse, rather than an acetone rinse after exposure to seawater.

The control sample with an air formed film showed a surface composition not significantly different from Figure 10. The surface was then sputtered and the peak to peak height for the elements carbon, nitrogen, oxygen, magnesium, and aluminum were measured with respect to depth (Figure 16). The film was relatively thin. Both carbon and nitrogen appear to be surface contaminants.

The sample that was immersed in seawater for thirty minutes shows a much thicker film (Figure 17). The thickness was approximately twice that of the air formed film. The carbon and nitrogen did not appear to be confined to the surface, but were distributed through the film. This would indicate the film was either porous or grew outward incorporating the carbon and nitrogen as it grew. The magnesium appeared to be similarly distributed, but as previously stated the levels were too low to draw conclusions.

The sample exposed to seawater for 11 hours had a film thickness between 30% and 40% greater than that of the 30 minute exposure specimen (Figure 18). The carbon and nitrogen were similarly incorporated into the film. The magnesium signal is not above the background noise. This data indicates the film grows

rapidly when initially immersed in seawater. The film appeared well formed by the end of the first thirty minutes.

An important objective of this research was the correlation of SAM data with the electrochemical data from the SPM. This was accomplished by analysing the same sample with both the SPM and SAM. Figure 19 shows the SPM plot for a sample which was immersed in seawater. Unfortunately, at the time the sample was removed from the solution there were no active pits on the surface. SAM secondary electron images did show the presence of inactive pits on the surface. A SAM spectrum was taken at the edge of one of these pits (Figure 20). The spectrum shows the surface to be composed almost entirely of aluminum oxide. This is possibly due to the rapid precipitation of aluminum oxide from the pit. At one pit diameter from the pit (200 microns) a second spectrum was taken (Figure 21). This site shows a composition more typical of a random site. If it is assumed the sulfur is present entirely as sulphate from seawater which dryed on the surface, the amount of magnesium which was in excess of that due to the drying of seawater can be determined. This method indicates approximately 19% of the surface metallic cations were magnesium. On this sample at points far from pits the magnesium concentration ranged from 3% to 12%. This is not, however, sufficient data to determine if the concentration of magnesium was significantly higher near pits.

A second sample was placed in a seawater solution which had been contaminated with copper ions. The SPM plot of the sample

when removed from the solution is shown in Figure 22. There was a very strong anodic site at the upper left hand corner of the specimen. This was associated with a shiny spot of the surface. This type of corrosion cell has been observed only in solutions which contained copper. The central part of the specimen produced the SAM spectrum in Figure 23. The surface was 10% magnesium and 2% copper. A SAM spectrum was taken at the lower edge of the specimen (Figure 24). The surface composition at this point was 10% magnesium and 4% copper. When a spectrum was taken in the area of the anodic activity (Figure 25) the surface was found to be 27% magnesium and 8% copper. Both of these elements showed a significant increase in surface concentration as the anodic site was approached.

On a specimen's surface cathodic activity should increase as an anode is approached, since the solution resistance increases with distance from the anode. If an element is precipitated by a cathodic reaction one would expect its concentration to increase as an anodic site is approached. It is well known that copper, being more stable than aluminum, is precipitated by an exchange reaction onto the aluminum surface. Once precipitated the copper depolarizes the oxygen reduction reaction. Copper exhibits this increase in concentration near anodes. Magnesium also exhibits this behavior, as clearly demonstrated by Figure 26, a magnesium map of the surface in Figure 14. It was not at all clear how magnesiun which is less stable than aluminum can precipitate and

contribute to the cathodic reaction on an aluminum surface. However, Dexter (1979B) has shown that magnesium contributes significantly to the total cathodic activity on an aluminum surface in seawater.

A possible explanation of how magnesium can act as a cathode is found by studing its adsorbtion reaction on an alumina surface. The following adsorbtion reaction for magnesium on alumina was proposed by Huang and Stumm (1972):

$$Al\text{-}OH + Mg^{+2} \rightarrow Al\text{-}O\text{-}Mg + H^{+}$$

Where Al- is a surface site on the alumina. If instead of producing H^{+} the reaction produced H_2 with the consumption of electrons the following cathodic reaction would result:

$$Al\text{-}OH + e^{-} + Mg^{+2} \rightarrow Al\text{-}O\text{-}Mg + 1/2H_2$$

This reaction would explain how magnesium ions could be cathodic to aluminum despite metallic magnesium's more active potential.

Computer Analysis

The computer analysis for this project was limited to modeling the activity of copper ions in seawater with varying concentrations of organics. The program used was HALTAFALL (Ingri, et al. 1967). Although modifications were made to the program, it could not be made to accept more complex scenarios. The solution modeled consisted of the major elements of seawater at seawater concentrations with copper as the only minor element. A hypothetical organic was added at concentrations similar to those in both natural seawater and an organic fouling film. The data indicates that organic films could play an important role in determining the activity of copper ions at surfaces in seawater (Figure 27).

At the present time we are implementing the program MINEQL II (Wesfall, et al.) with the Stanford adsorption package (James and Parks). This program will allow the modeling of the speciation of complex solutions and the adsorbtion of ions on solid surfaces. The adsorbtion of ions onto an aluminum surface in seawater is to be modeled. These results are to be compared to those obtained by SAM analysis.

Conclusions

This research has shown that the oxide films which form on an aluminum surface in seawater are significantly different from those formed in laboratory saline solutions. The most outstanding difference being the presence of significant magnesium concentrations on the surface. These concentrations can reach at least 27% near strong anodes. The distribution pattern of the magnesium indicates it adsorbs cathodically. The cathodic nature of magnesium has been confermed by Dexter (1979). It is hypothysized that the cathodic reaction is related to the adsorbtion chemistry by the reaction:

$$Al\text{-}OH + e^- + Mg^{+2} \rightarrow Al\text{-}O\text{-}Mg + 1/2H_2$$

Where Al- is a surface site on the oxide.

When aluminum is placed in seawater contaminated with copper ions, the copper adsorbs onto the surface. The copper deposits vary widely in size. Large amounts of copper appear to be in the finely dispersed phase. This copper could have a cathodic strength comparable to the larger copper particles noted in earlier research (Craig 1974). There was no evidence for preferential cathodes on aluminum with strenghts larger than a few per cent that of anodes.

The computer modeling of seawater has shown that organics in seawater should affect the activity of copper ions in solution near

any surface. These films could significantly affect the corrosion of aluminum in seawater which has been contaminated with copper.

Further Research

This project is to be continued with funding from the Sea Grant National Program in Marine Corrosion. During the next year the Scanning Potential Microprobe lab will be upgraded with the addition of a constant temperature bath, a pH meter, and a salinometer.

Computer adsorbtion models for aluminum in seawater will be run using the program MINEQL with the Stanford adsorbtion package.

Experiments will be devised and executed to test the mechanism of cathodic activity proposed for magnesium on aluminum in this report.

Much more correlated SPM-SAM data will be collected and analysed, including elemental mapping and depth profiles.

How aluminum surface compositions and electrochemistry vary under differing conditions of temperature, pH, salinity, and potential are to be investigated. These experiments will utilize the equipment budgeted for in next year's grant and the potentiostat (Aardvark model V-2LR) obtained this year. The investigations of film composition verses potential have begun, but mechanical problems with the SAM prevented specimen analysis of the schedualed date. Mr. Smith is now certified to use the SAM after hours, so that the 1 to 2 month wait for daytime SAM use will be avoided in the future.

Acknowledgments

This research was completed with funding by the MIT Office of Sea Grant. A special thanks must go to Mr. Dean Horn for special help in obtaining this funding.

Mr. Hugh Isaacs of the Brookhaven National Laboratories gave technical assistance and allowed free access to the plans for his Scanning Potential Microprobe.

Dr. Peter Brewer of the Woods Hole Oceanographic Institution gave advice on the use of chemical speciation models and allowed use of his version of HALTAFALL.

Dr. Tony Garret-Reed and Mr. John Martin of the Center for Materials Science and Engineering gave instruction in the operation of the Scanning Auger Microprobe and helped operate the machine during these experiments.

Bibliography

Craig, H.L., "Kinetic Studies of Aluminum Pitting Reactions", Prodeedings U.R. Evans Conference on Localized Corrosion, Williamsburg, Va., 6-10 December 1971, 600, (1974).

Dexter, S.C., "Effect of Variations in Seawater Upon the Corrosion of Aluminum", Corrosion '79, Paper No. 232 (1979).

Dexter, S.C., University of Delaware, Private Communication, (1979).

Huang, C., Stumm, W., "Specific Adsorbtion of Cations on Hydrous δ-Al_2O_3", Journal of Colloid and Interface Science, 43, 409-420, (1972).

Ingri, N., Kabolowicz, W., Sillen, L., Warnquist, B., "High Speed Computers as a Suppliment to Graphical Methods-V", Talanta, 14, 1261-1286, (1967).

Isaacs, H.S., "Potential Scanning of Stainless Steel During Pitting", Proceedings U.R. Evans Conference on Localized Corrosion, Williamsburg, Va., 6-10 December 1971, 158, (1974).

James, R.O., Parks, G.A., "Application of the Computer Program "MINEQL" to Solution of Surface Chemistry", Unpublished Manuscript, (No Date).

MacDonald, N.C., Riach, G.E., Gerlach, R.L., "Applications of Scanning Auger Microanalysis", Research/Development, 27, 8, 42-50,48,50, (1976).

Morse, J.W., "Inorganic Scale Chemistry of OTEC Test Heat Exchanger Tubes From the Gulf of Mexico Biofouling and Corrosion Experiment", Final Report, ONR Contract NOOO14-78-6-0651, (1979).

Wesfall, J.C., Zachary, J.L., Morel, F.M.M., "MINEQL A Computer Program for the Calculation of Chemical Equlibrium Composition of Aqueous Systems", Technical Note 18, EPA Grant No. R-803738, (No Date).

Table 1

Scanning Auger Microprobe Elemental Sensitivities
(Approximate values)
(Abridged Table)

Al	0.068
Mg	0.149
Cu	0.24
O	0.41
S	0.71

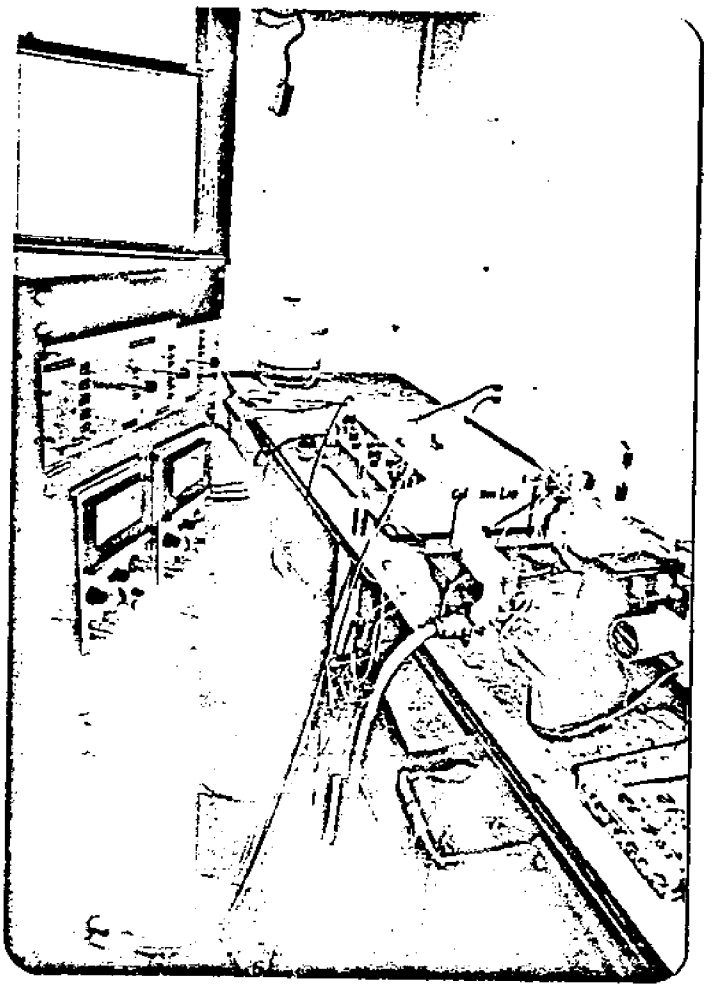

Figure 1

Scanning Potential Microprobe

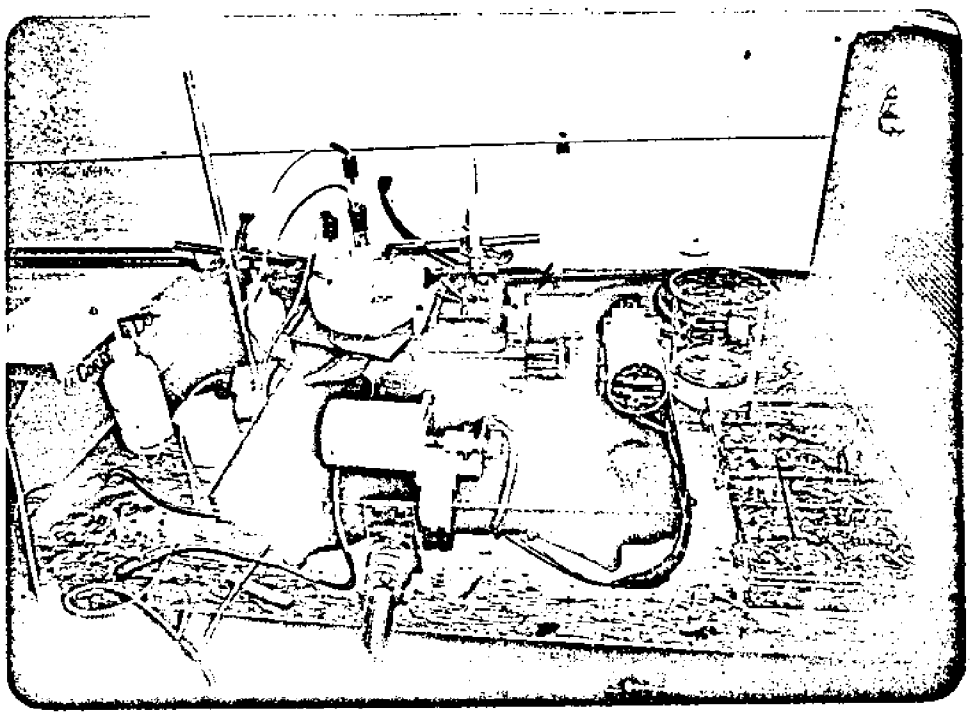

Figure 2

Scanning Potential Microprobe Stage

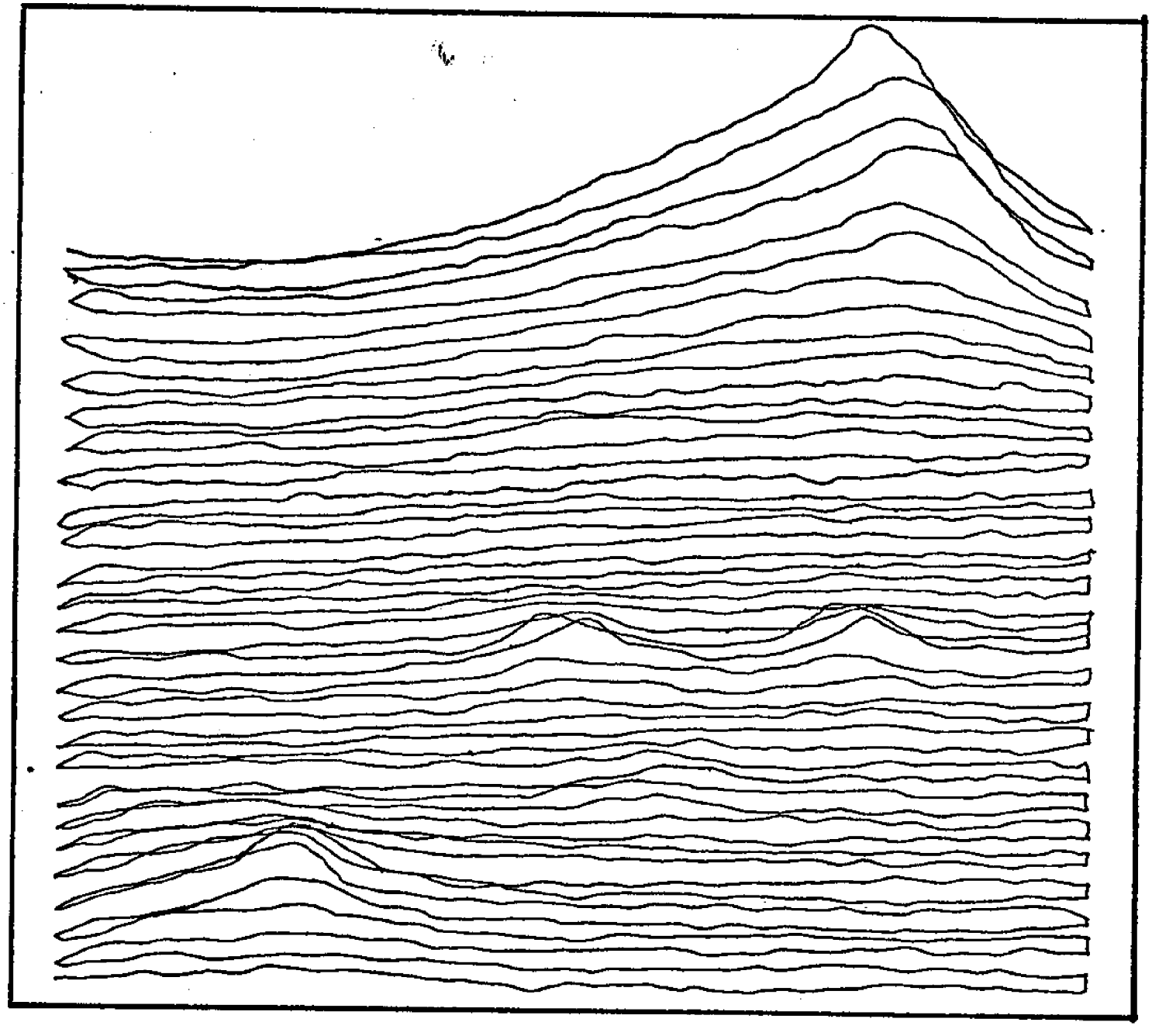

Figure 3

Scanning Potential Microprobe Output

Figure 4

Block Diagram of
Scanning Potential Microprobe

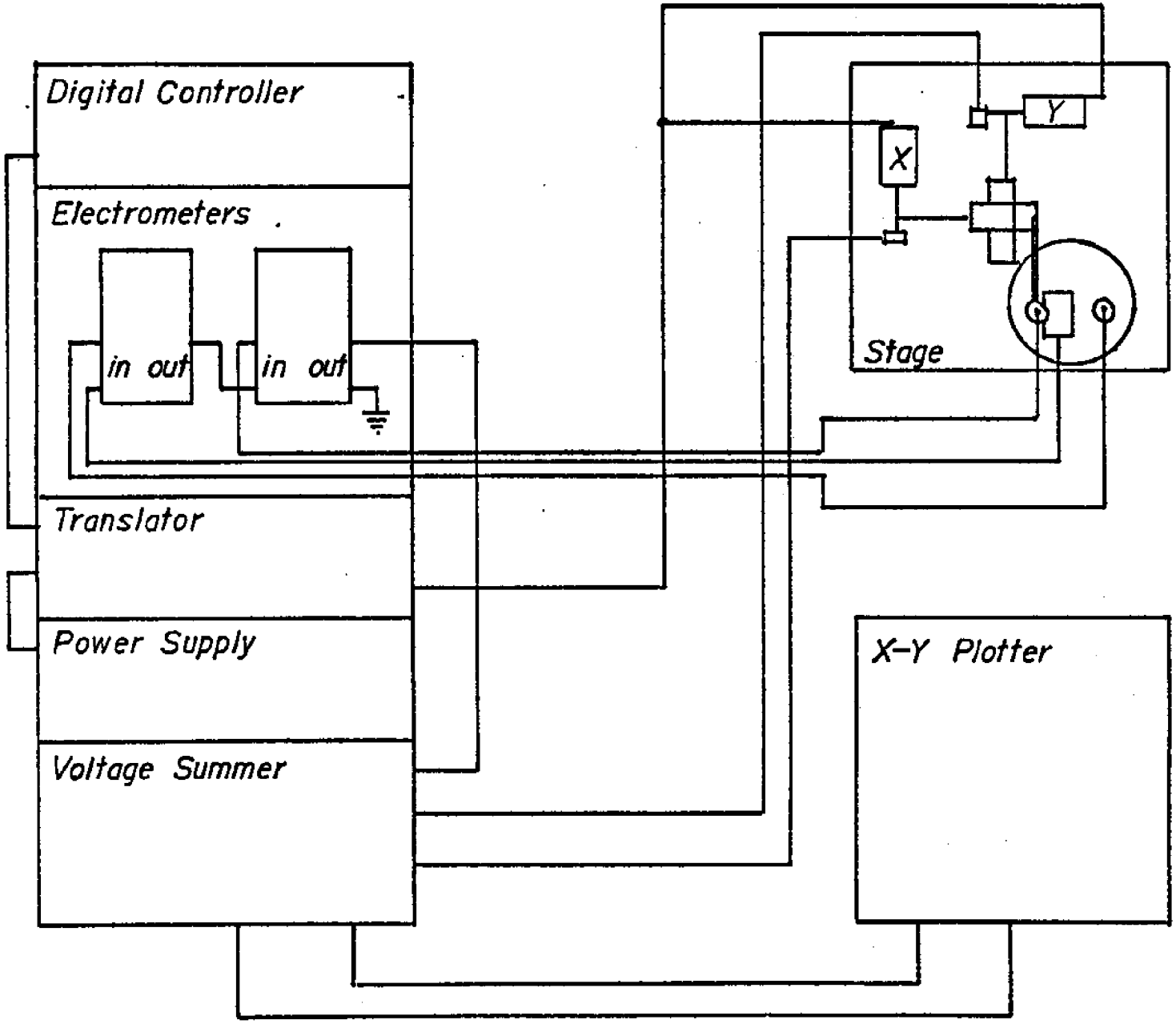

Figure 5

DIGITAL CONTROLLER SCHEMATIC

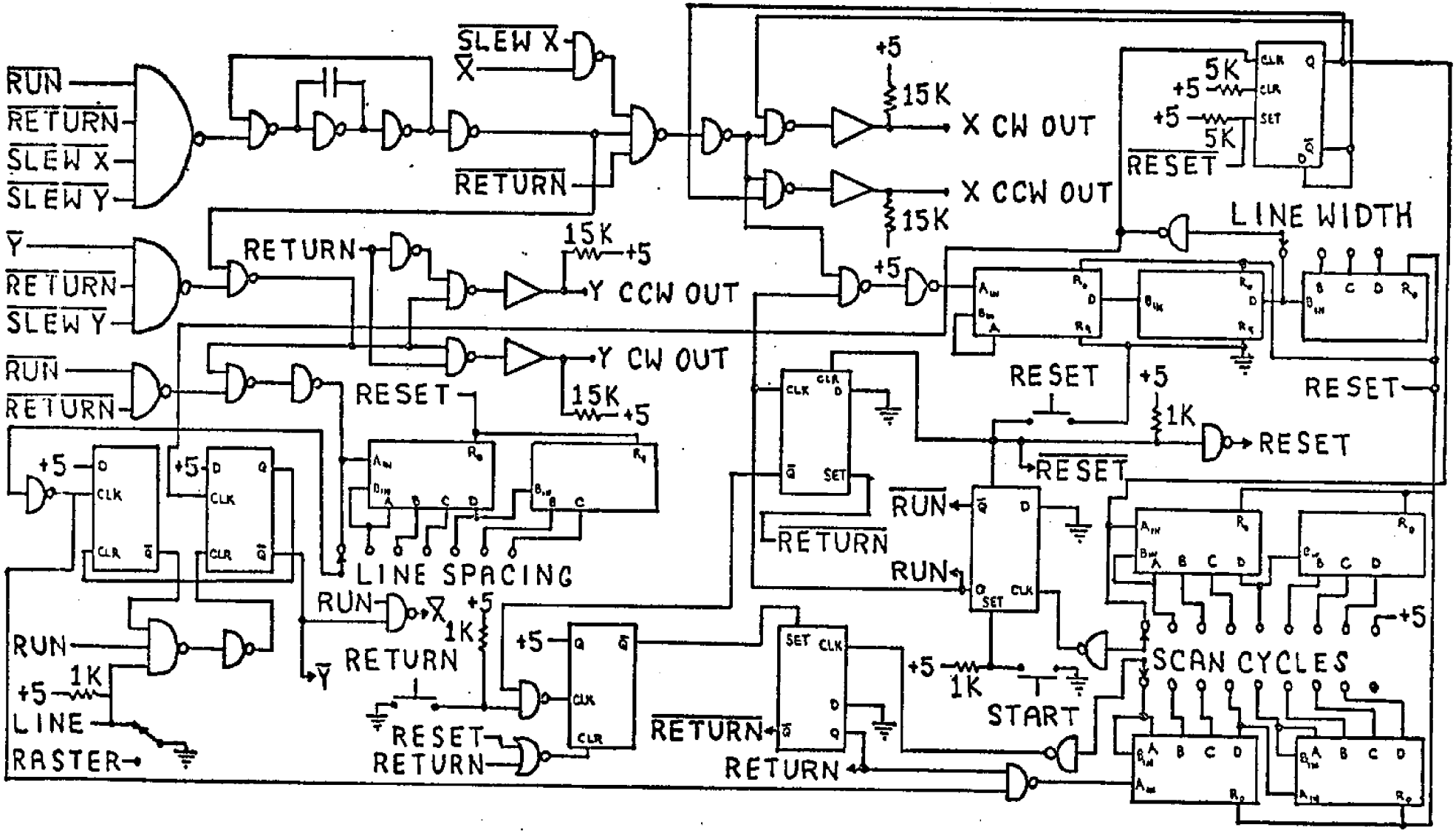

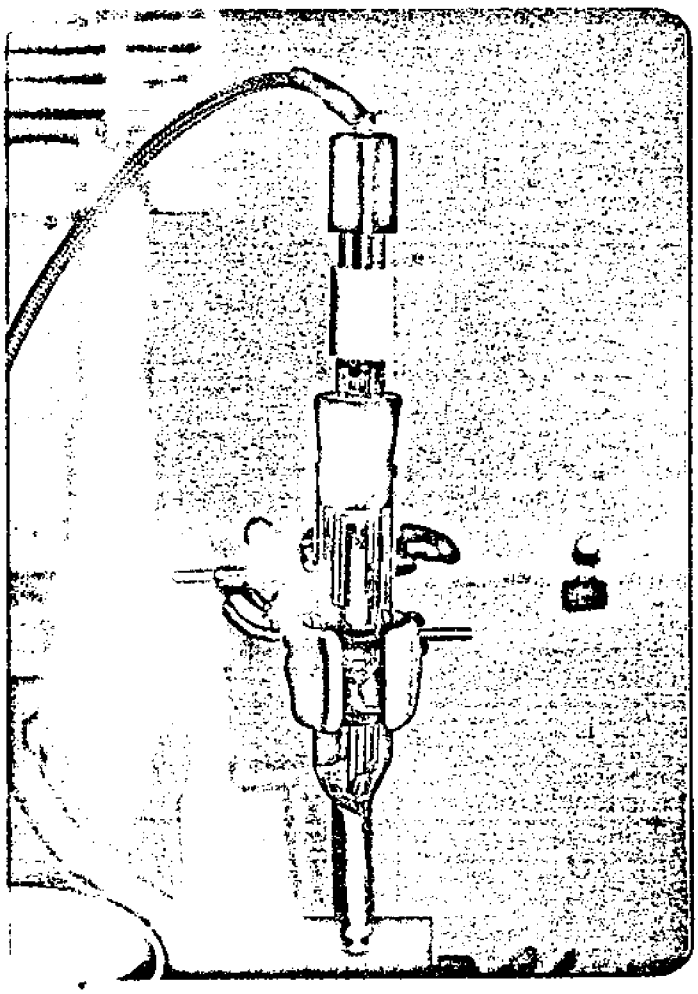

Figure 6

Scanning Potential Microprobe
Micro-Electrode

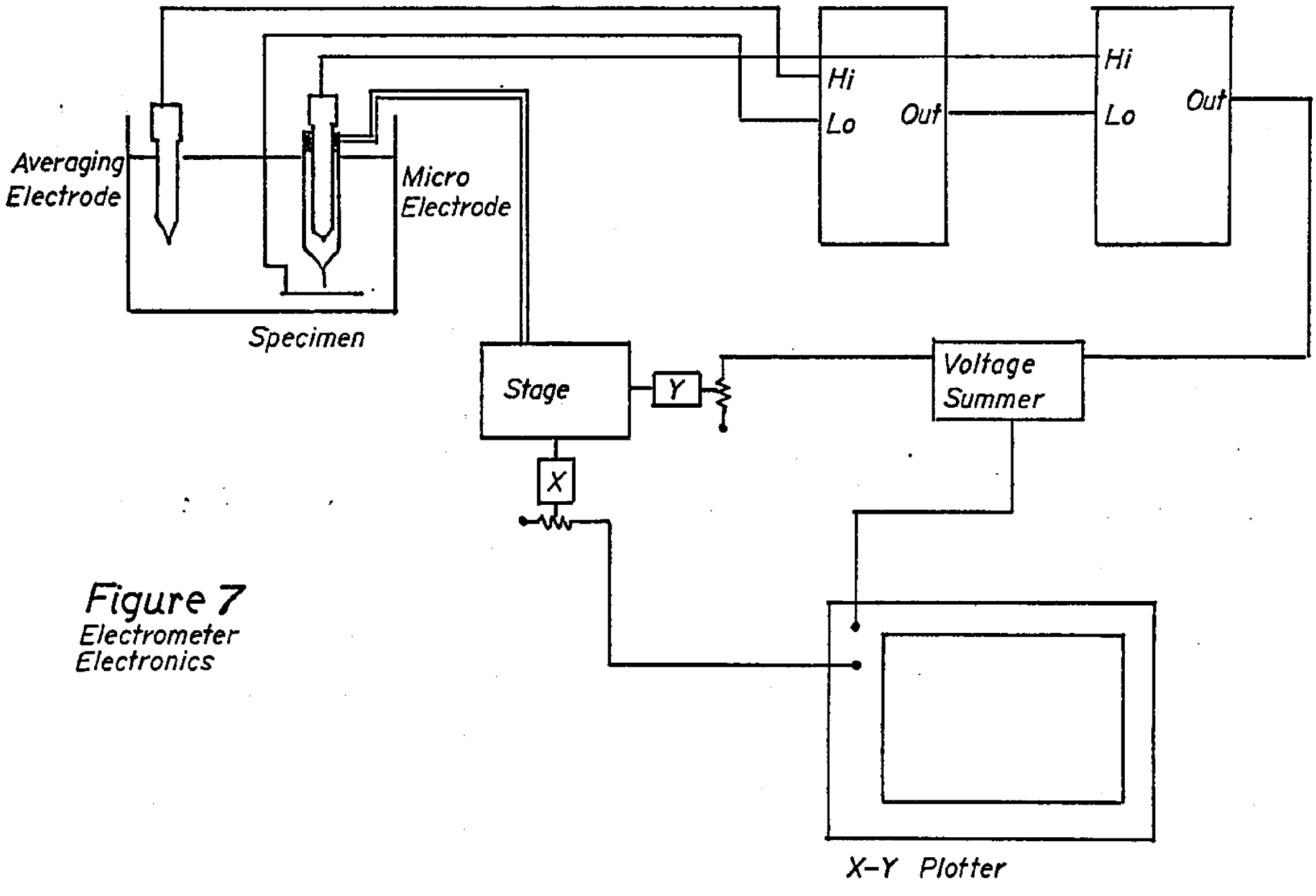

Figure 7
Electrometer Electronics

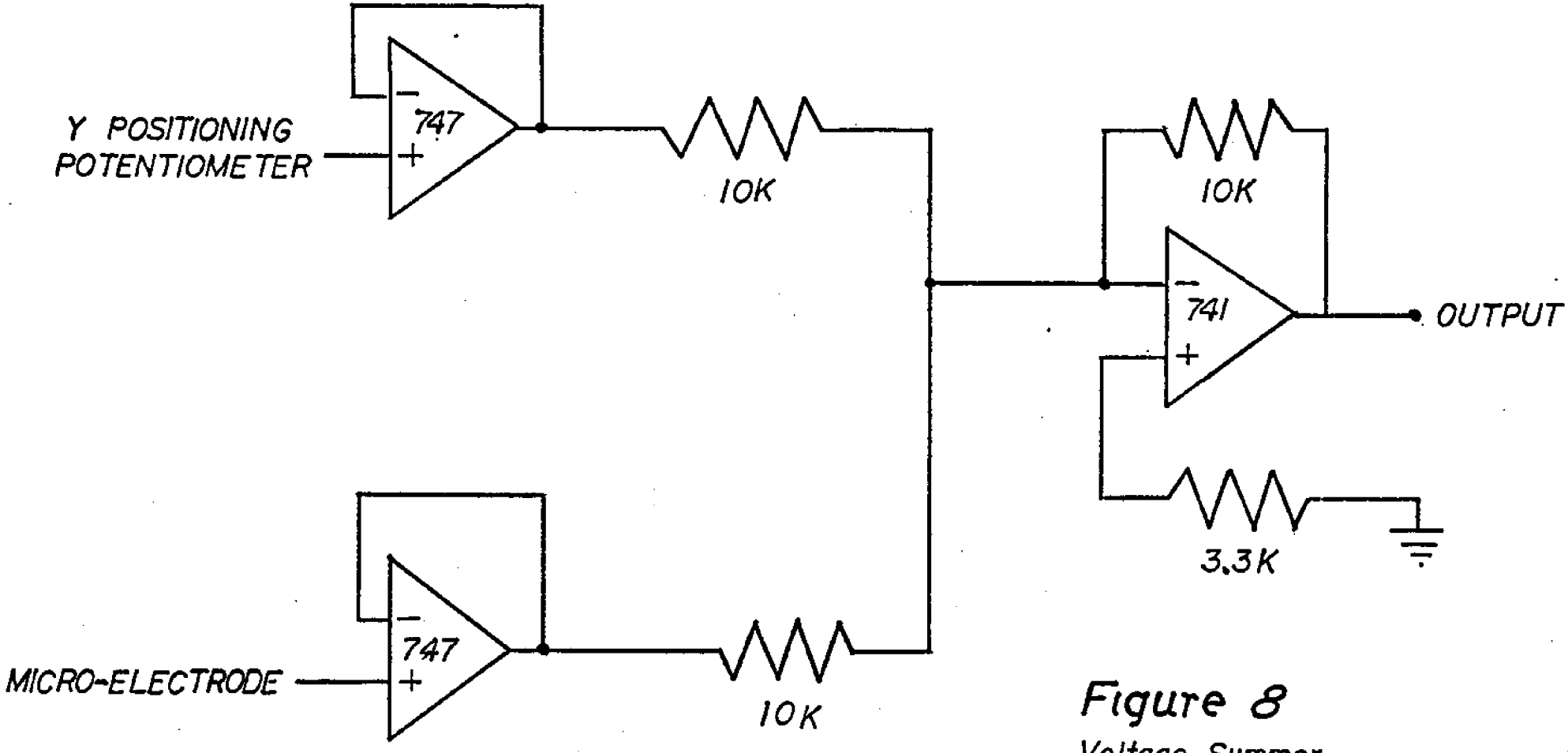

Figure 8
Voltage Summer
Schematic

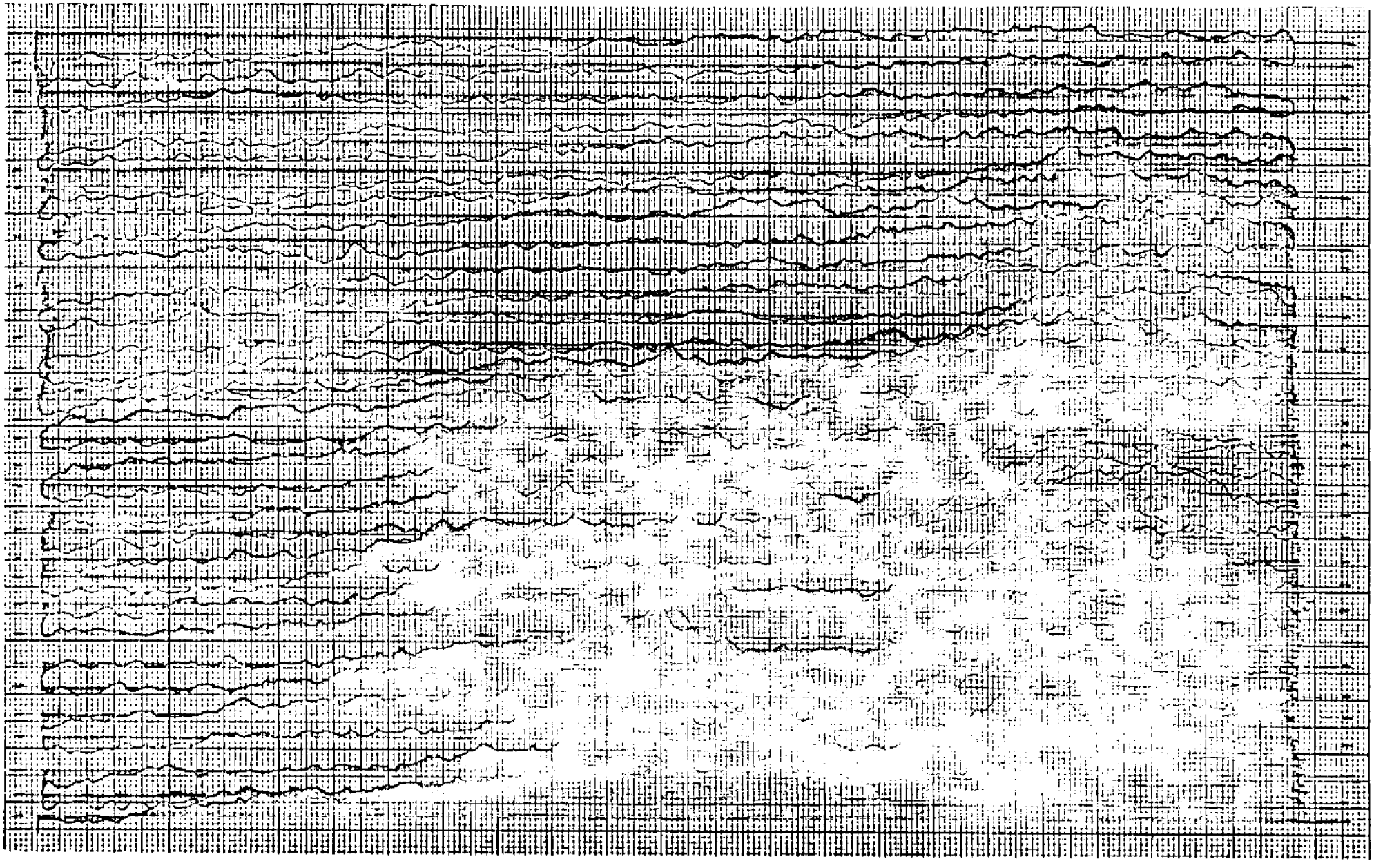

Figure 9
Color Aided Data
Scanning Potential Microprobe

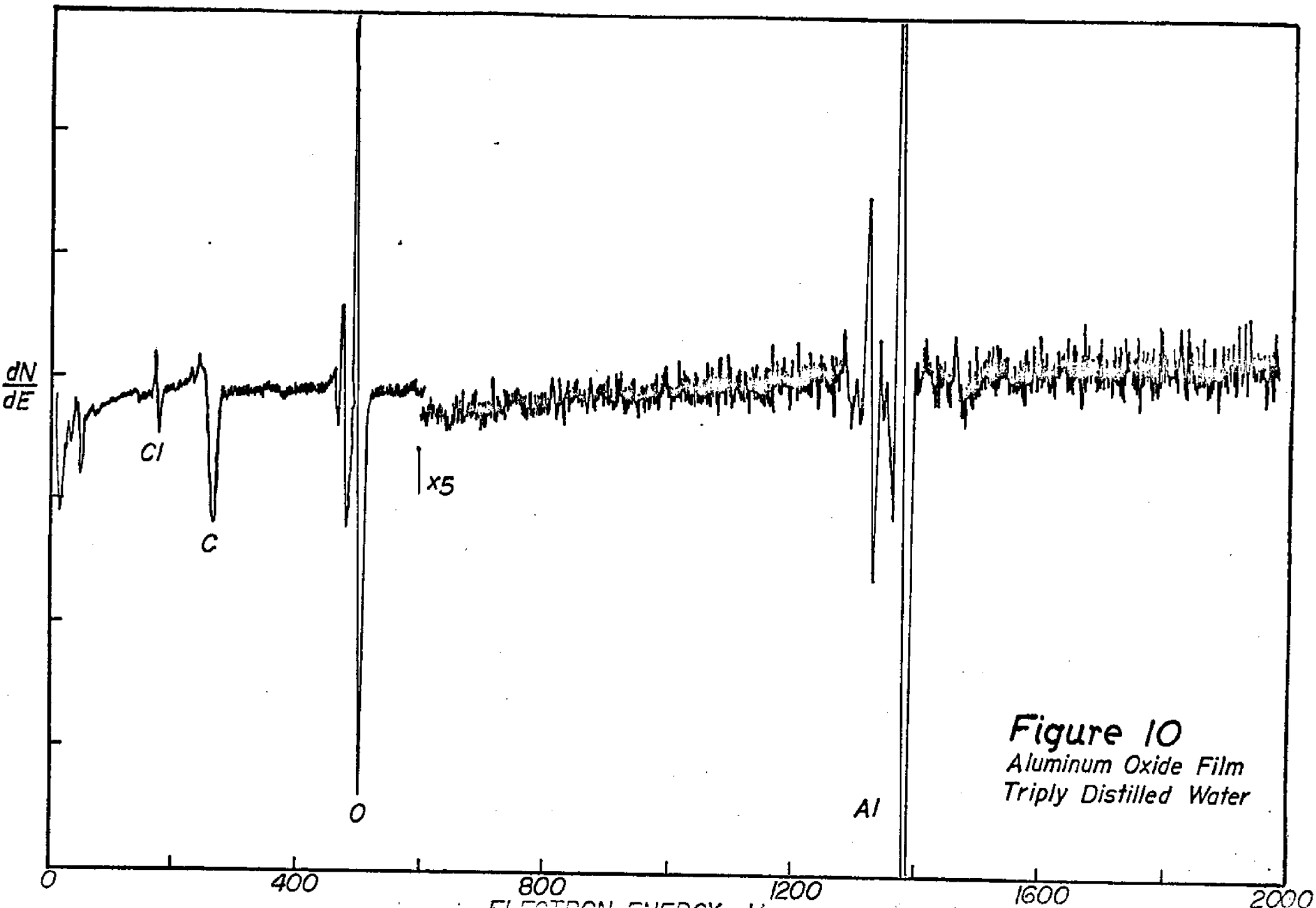

Figure 10
Aluminum Oxide Film
Triply Distilled Water

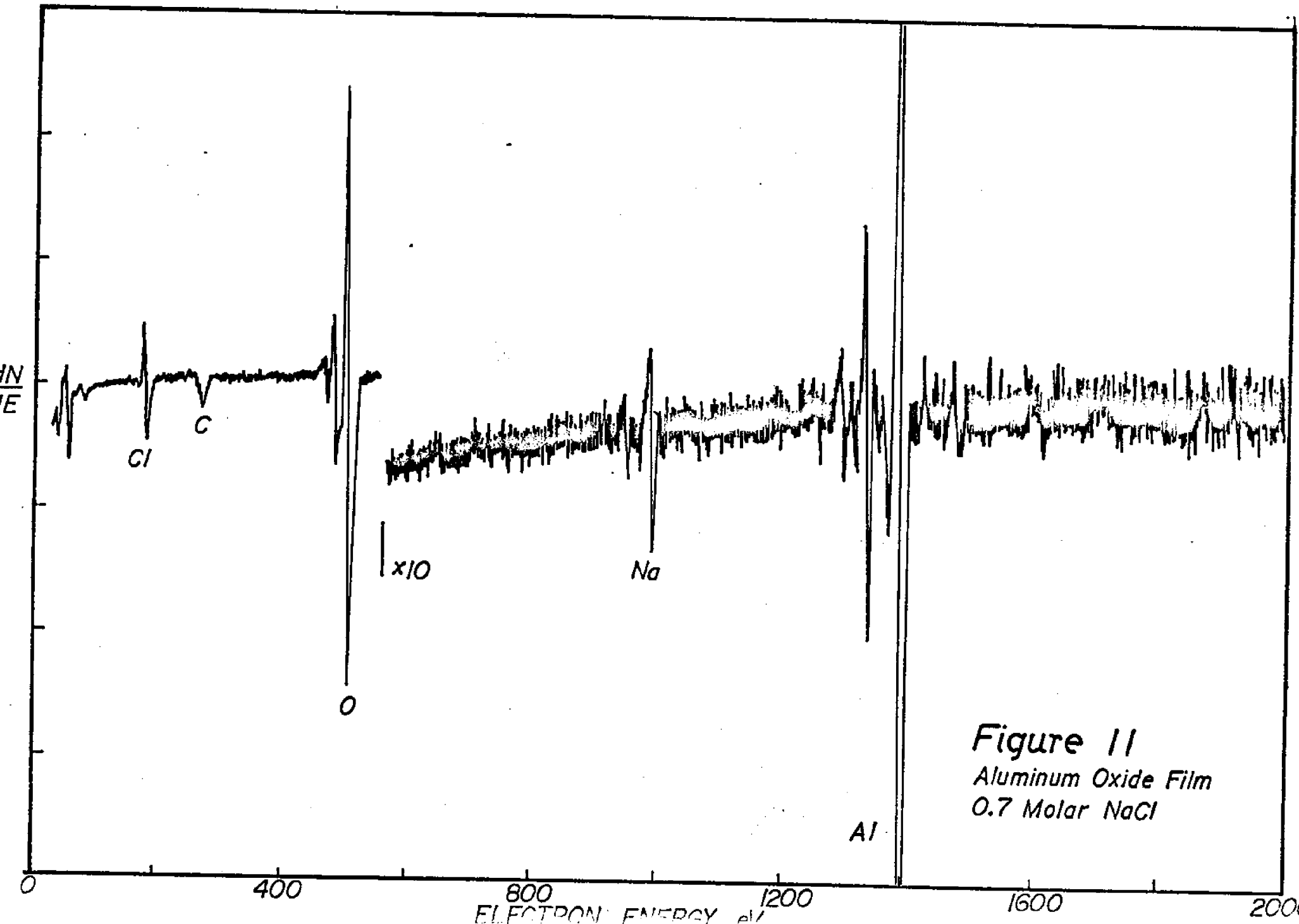

Figure 11
Aluminum Oxide Film
0.7 Molar NaCl

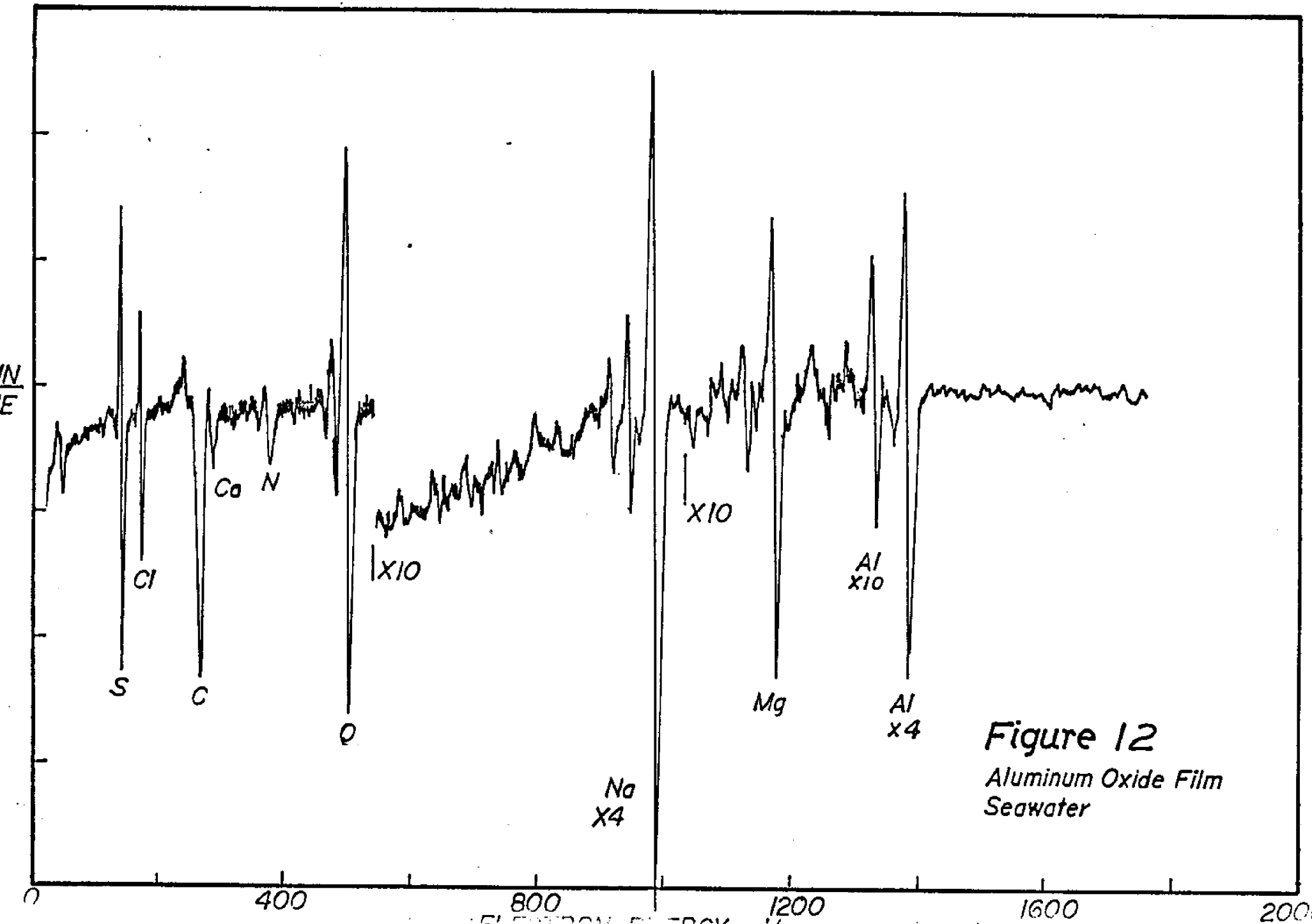

Figure 12

Aluminum Oxide Film
Seawater

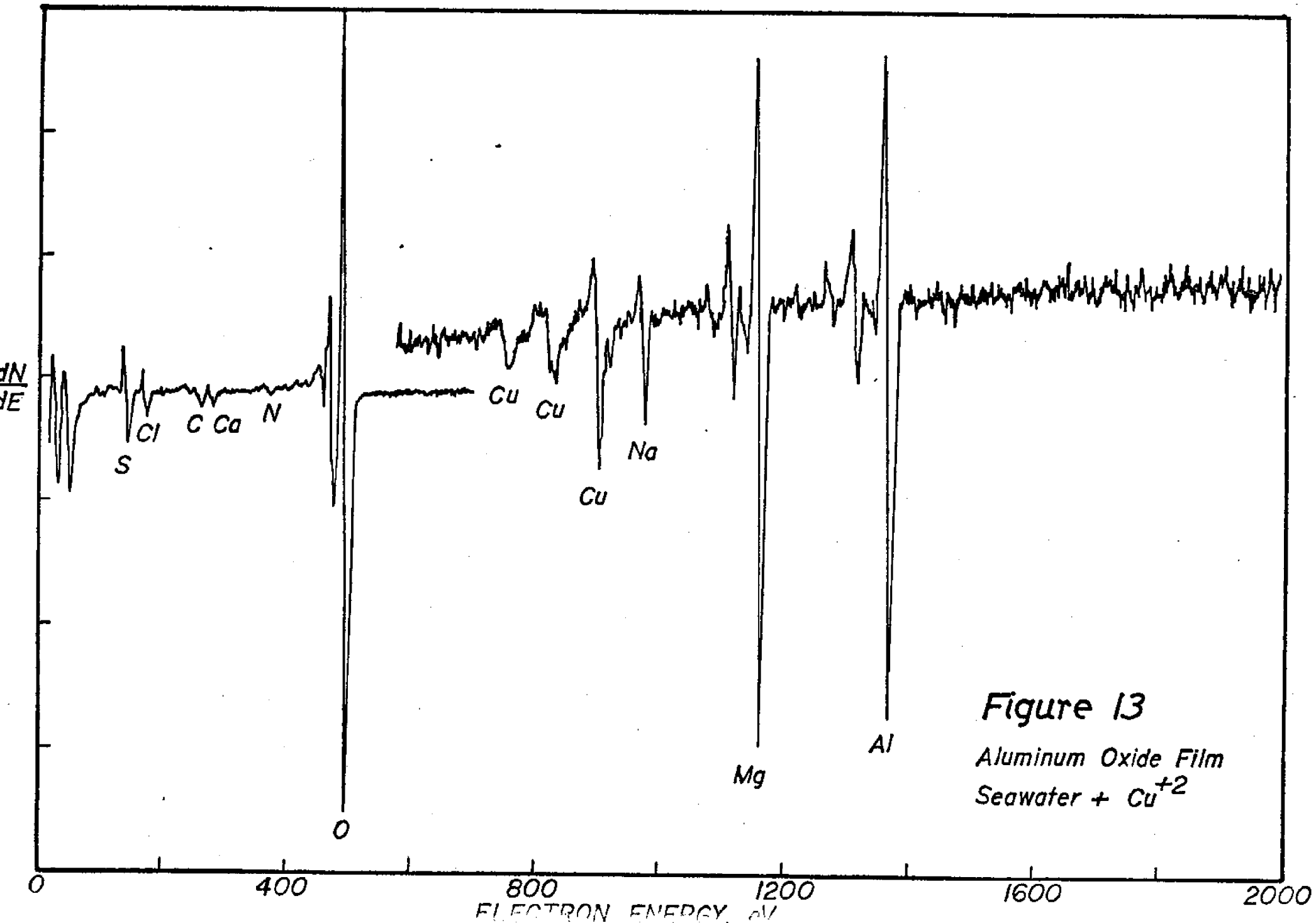

Figure 13

Aluminum Oxide Film

Seawater + Cu^{+2}

Figure 14
SED Image
Aluminum Surface
Seawater + Cu^{+2}.

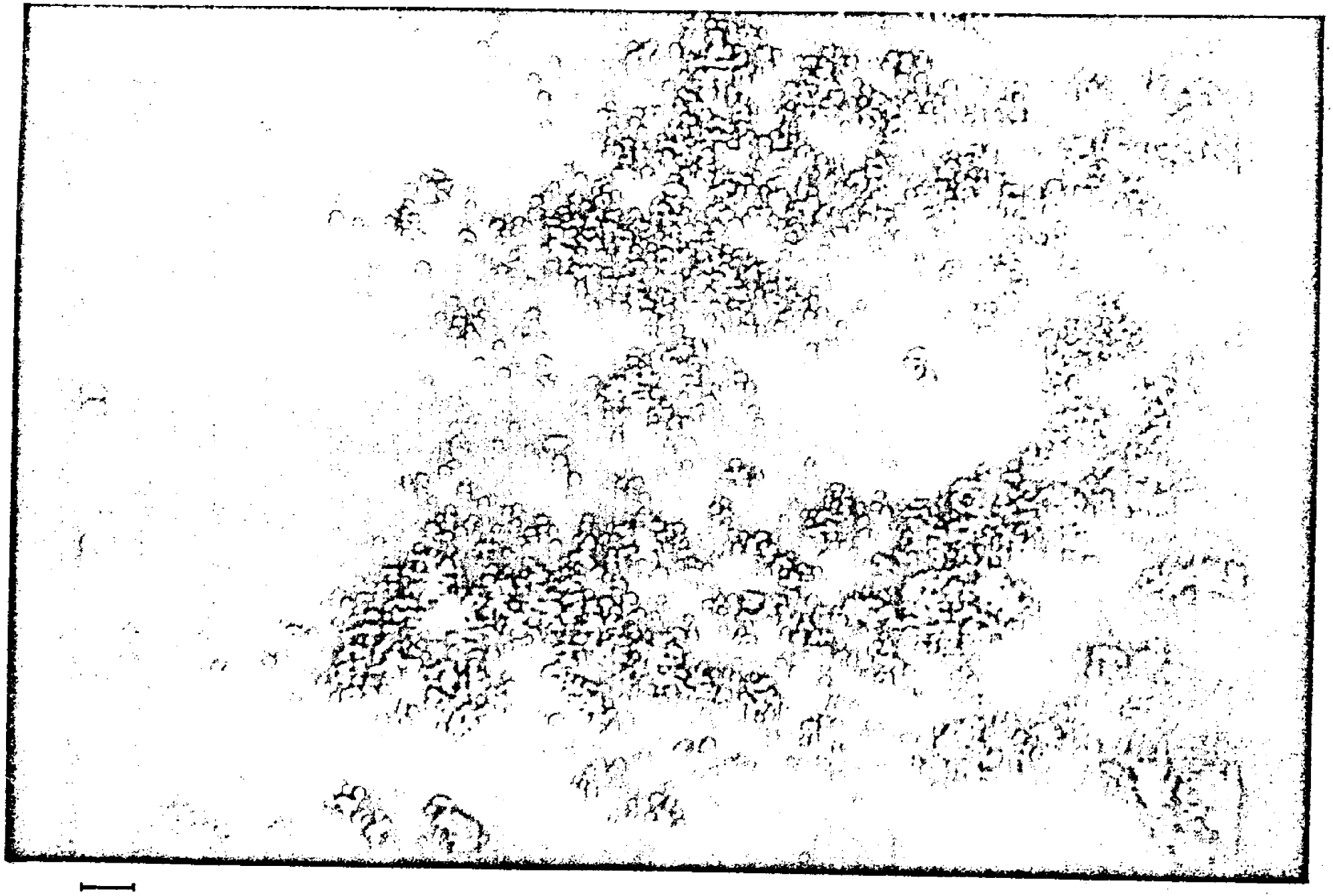

15 μm

Figure 15
Copper Map
Aluminum Surface
Seawater + Cu^{+2}

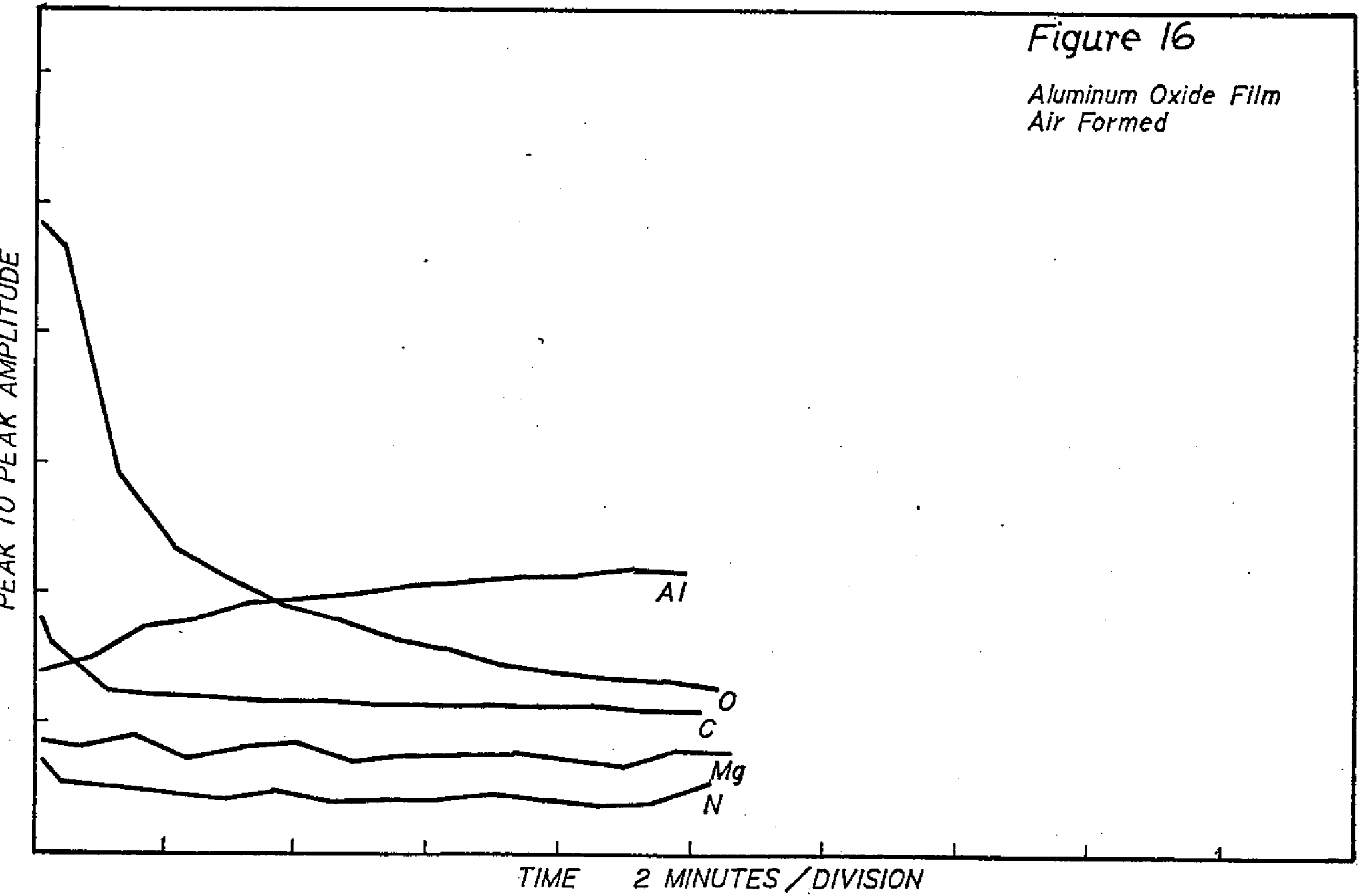
Figure 16
Aluminum Oxide Film
Air Formed
PEAK TO PEAK AMPLITUDE
Al
O
C
Mg
N
TIME 2 MINUTES / DIVISION

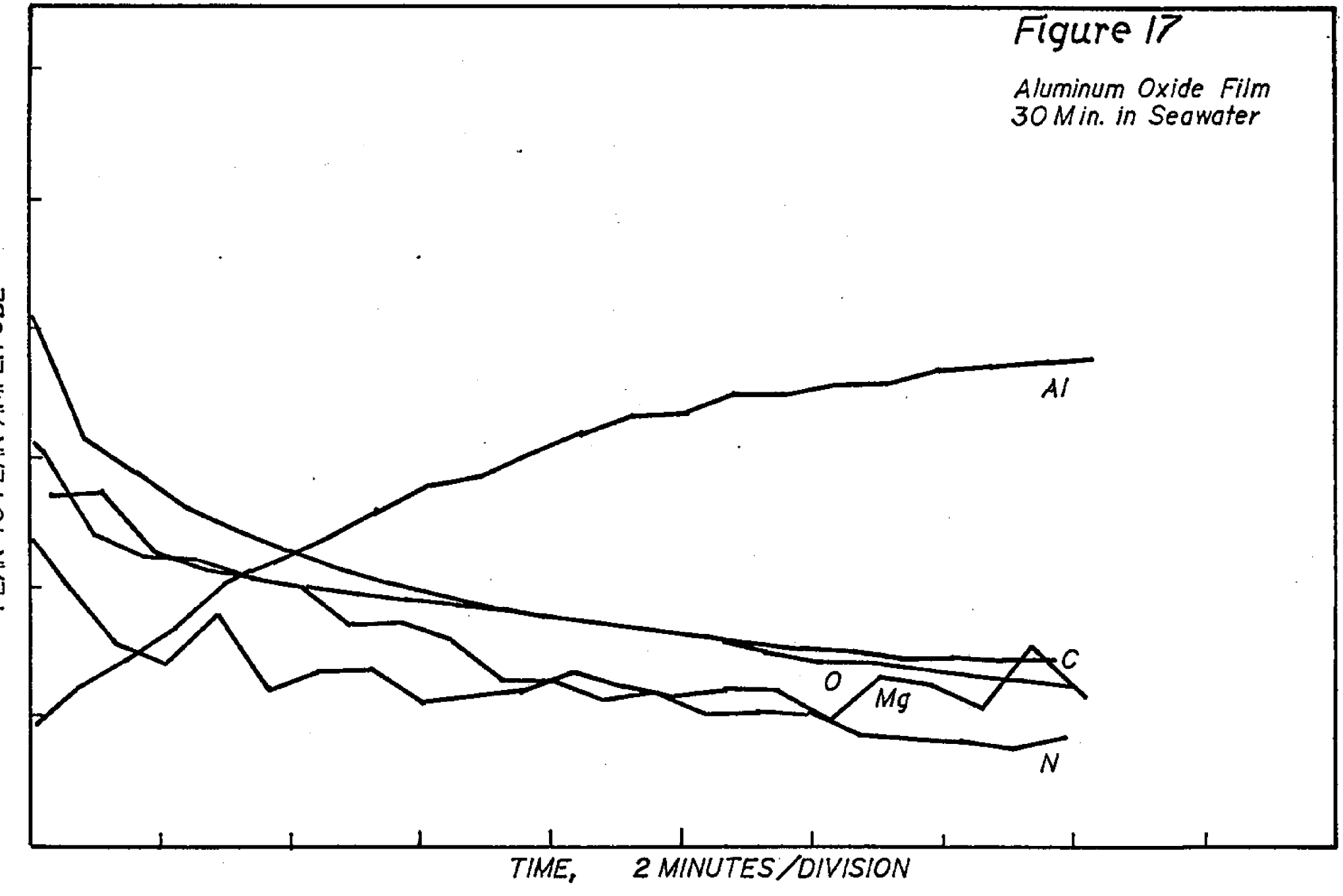
Figure 17
Aluminum Oxide Film
30 Min. in Seawater
Al
C
O
Mg
N
TIME, 2 MINUTES/DIVISION

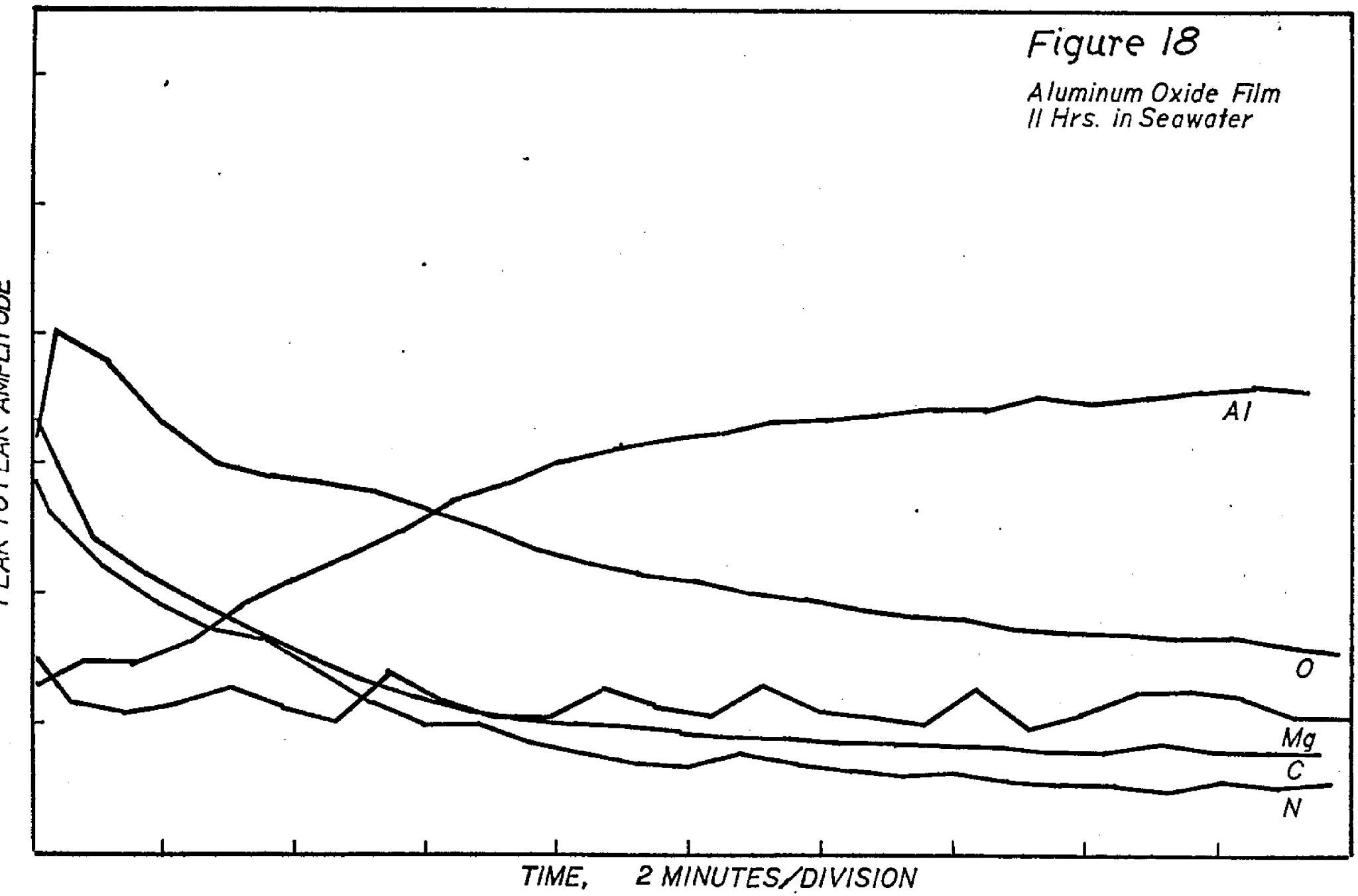
Figure 18
Aluminum Oxide Film
11 Hrs. in Seawater
PEAK TO PEAK AMPLITUDE
Al
O
Mg
C
N
TIME, 2 MINUTES/DIVISION

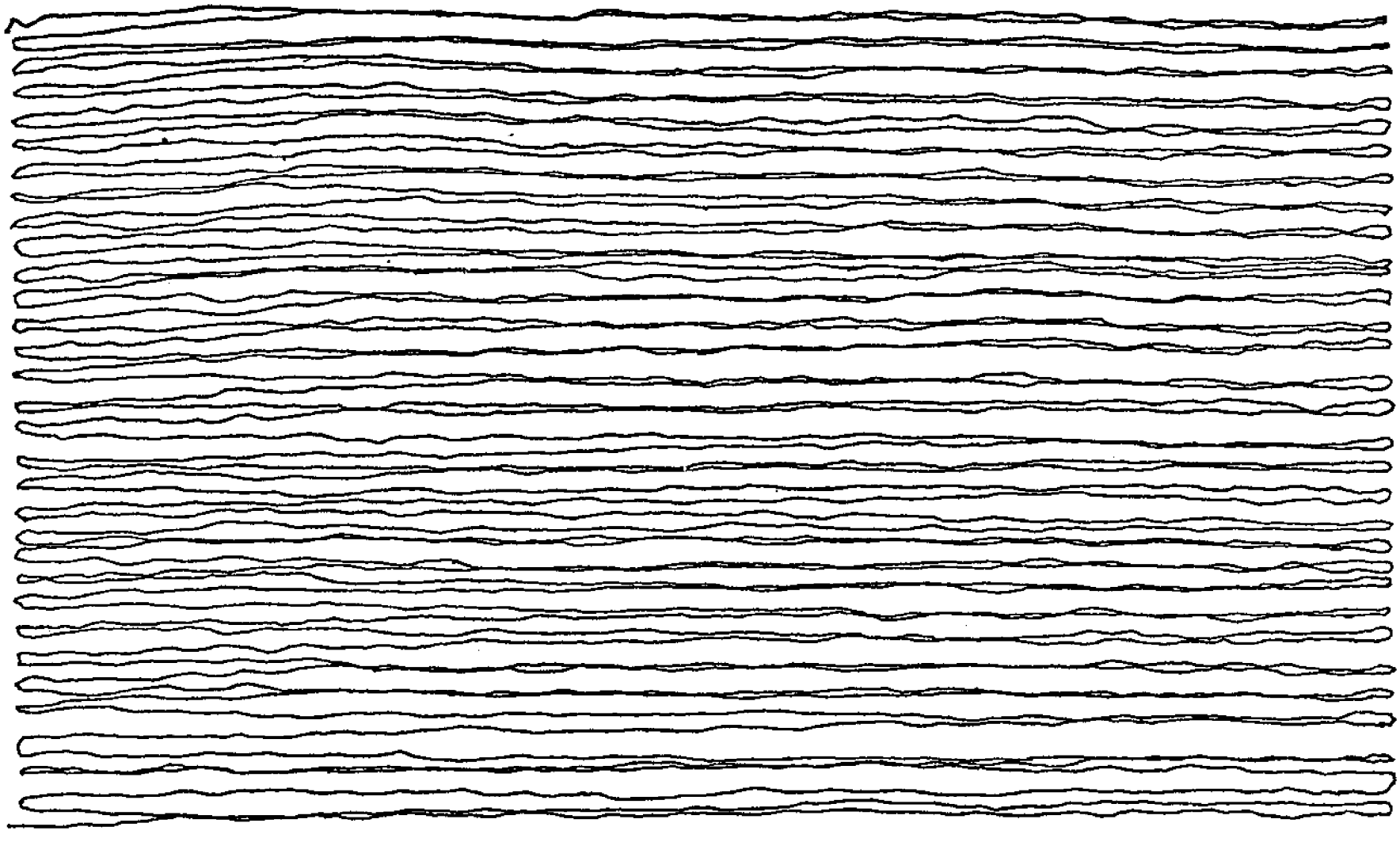

Figure 19
SPM Data
Seawater

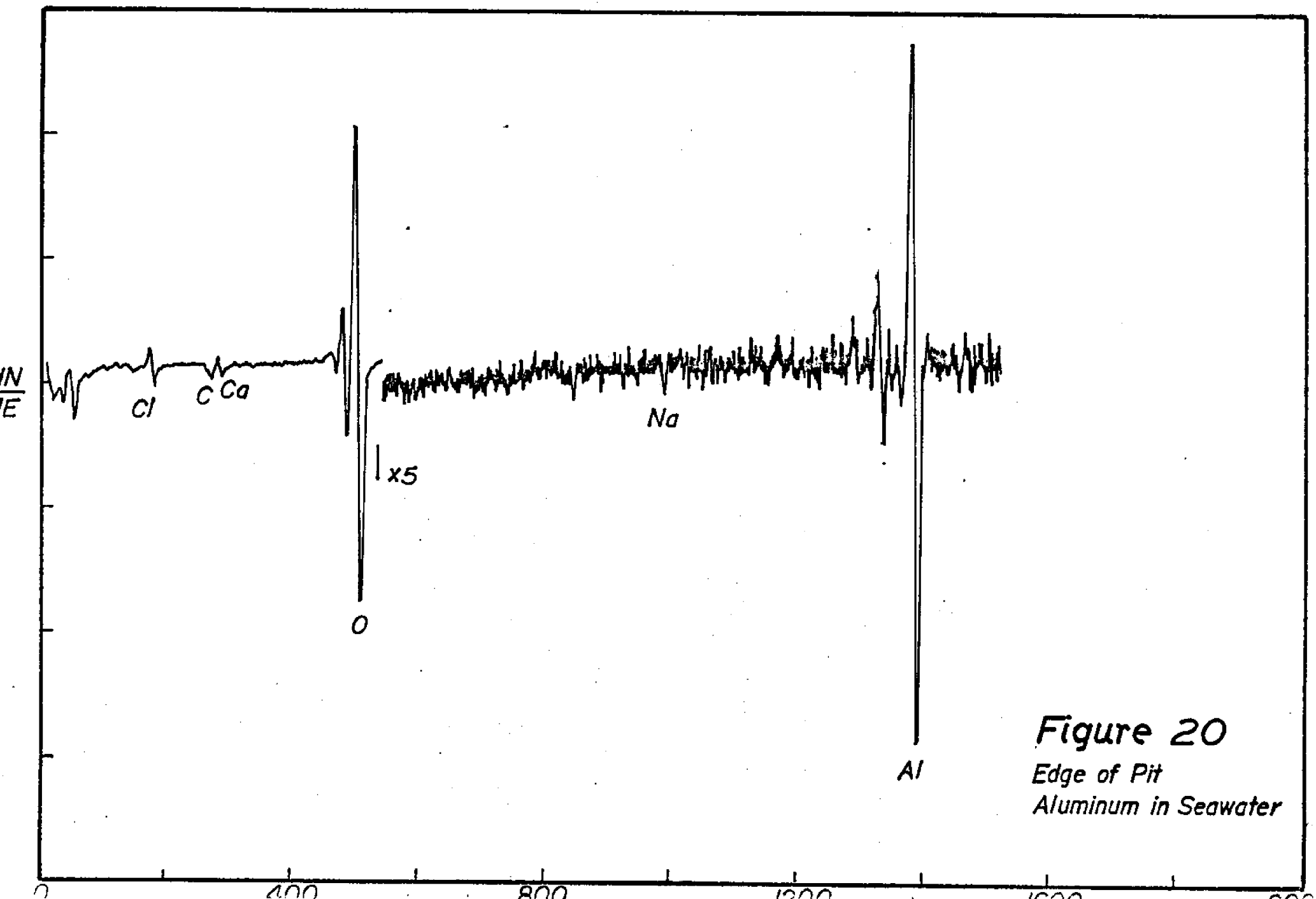

Figure 20

Edge of Pit

Aluminum in Seawater

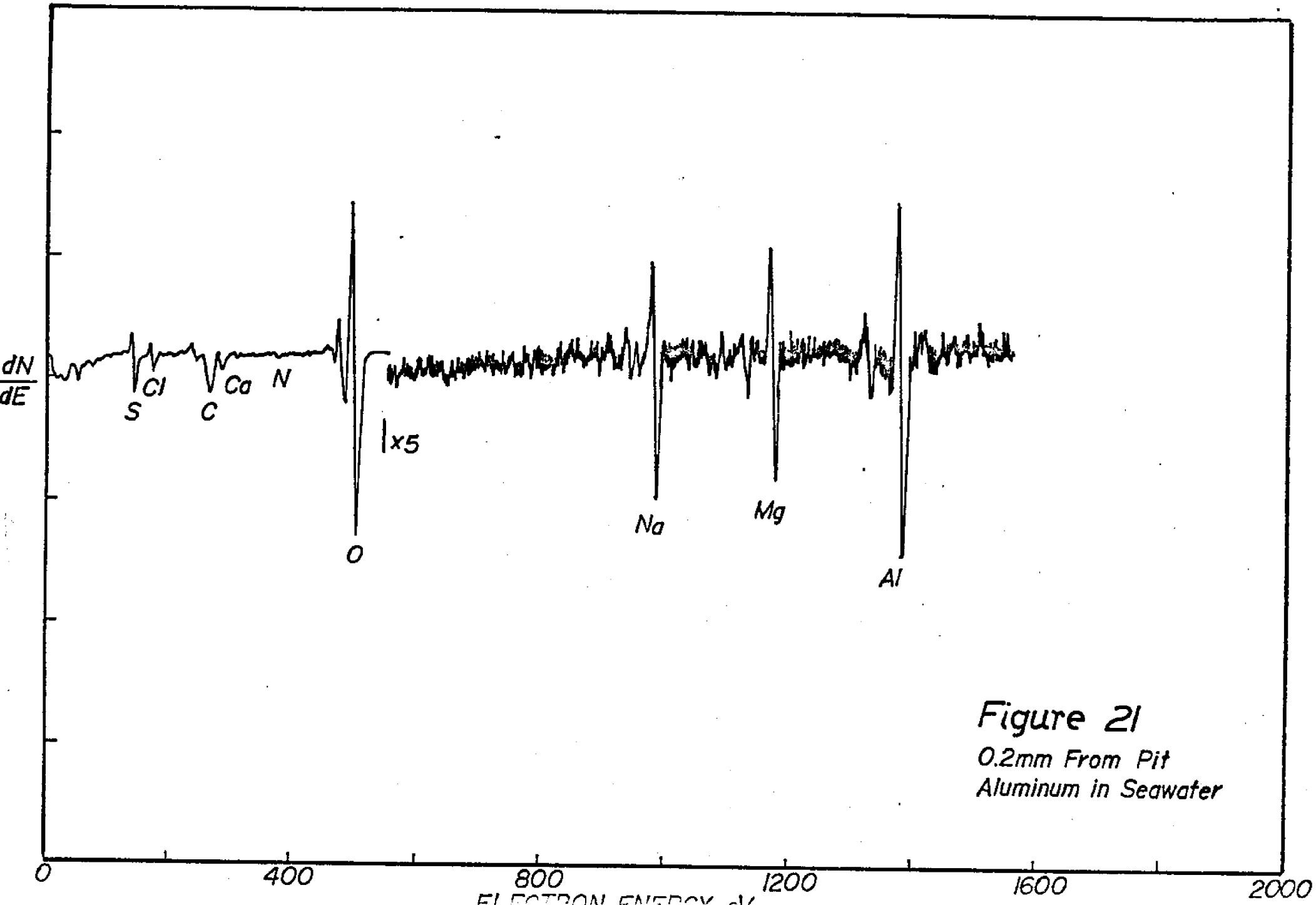

Figure 21

0.2mm From Pit
Aluminum in Seawater

Figure 22

SPM Data
Seawater + Cu^{+2}

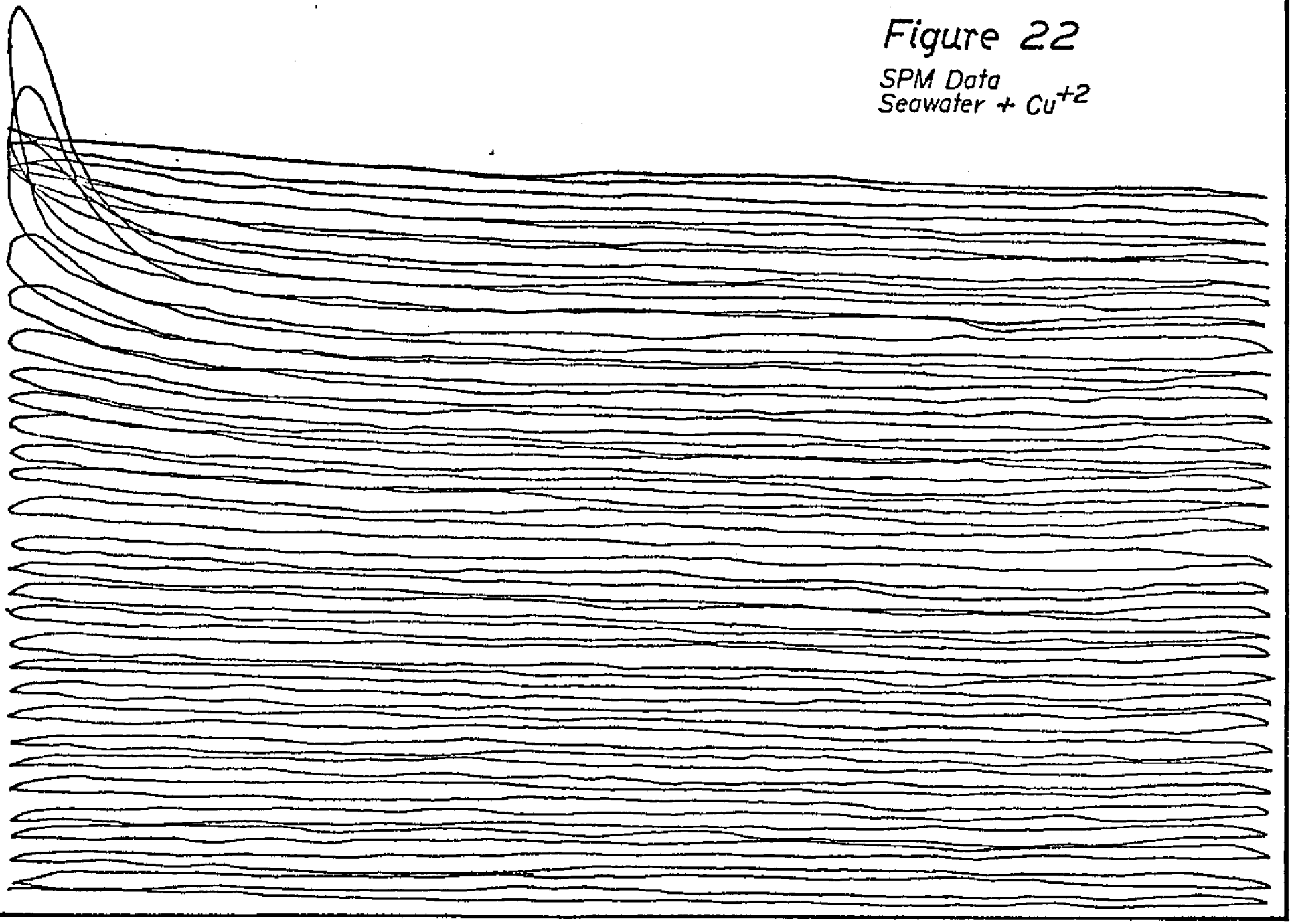

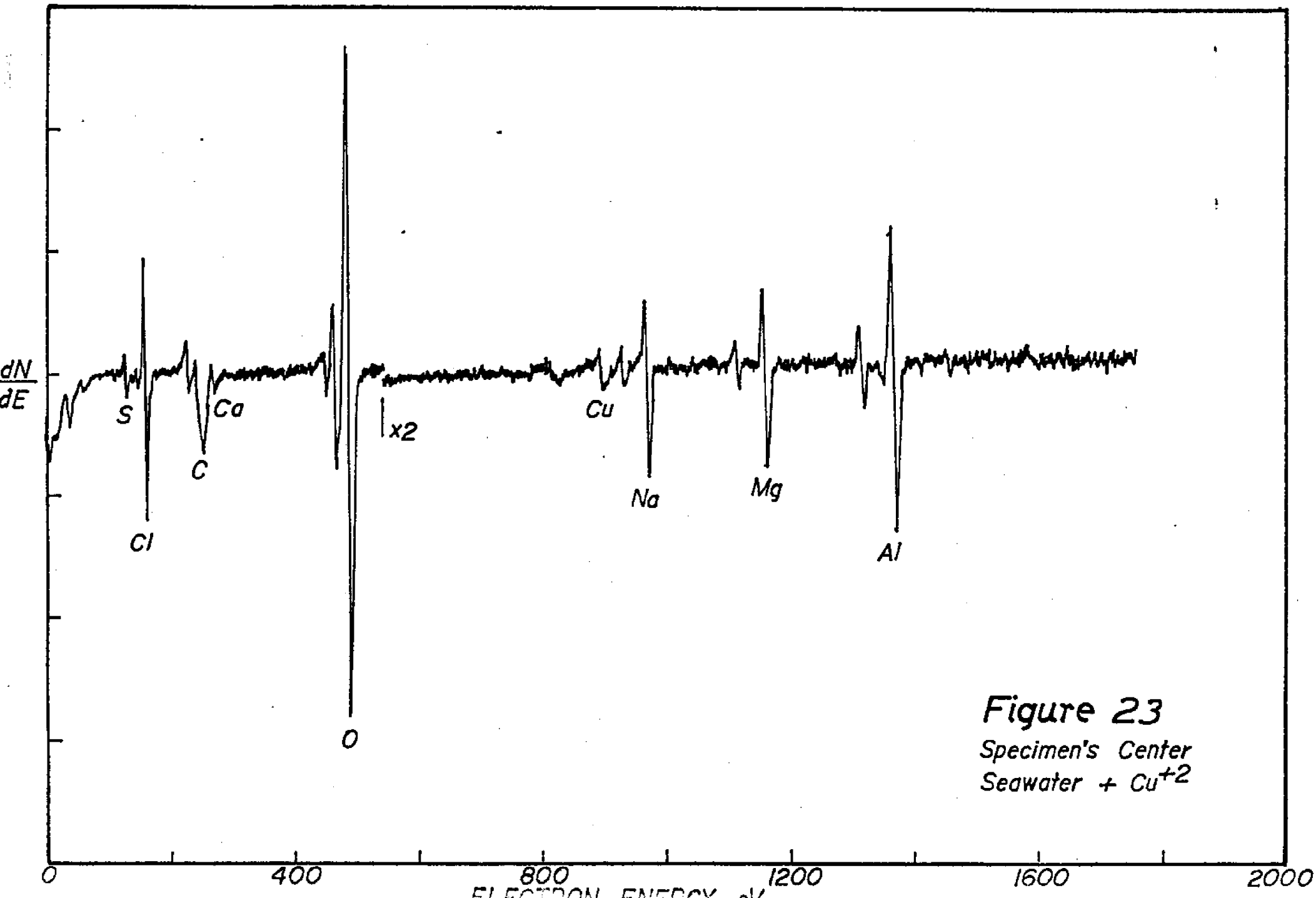

Figure 23
Specimen's Center
Seawater + Cu^{+2}

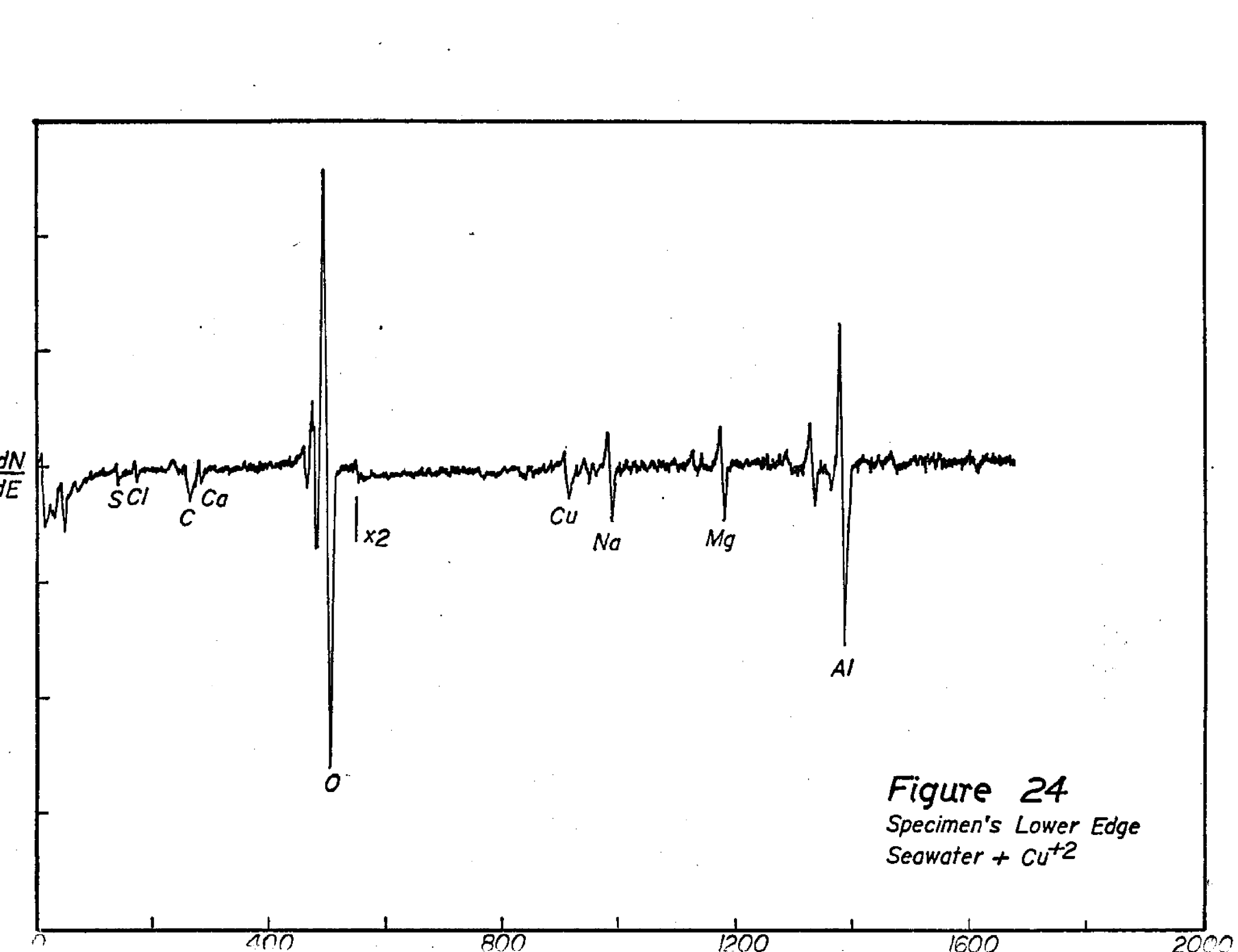

Figure 24
Specimen's Lower Edge
Seawater + Cu^{+2}

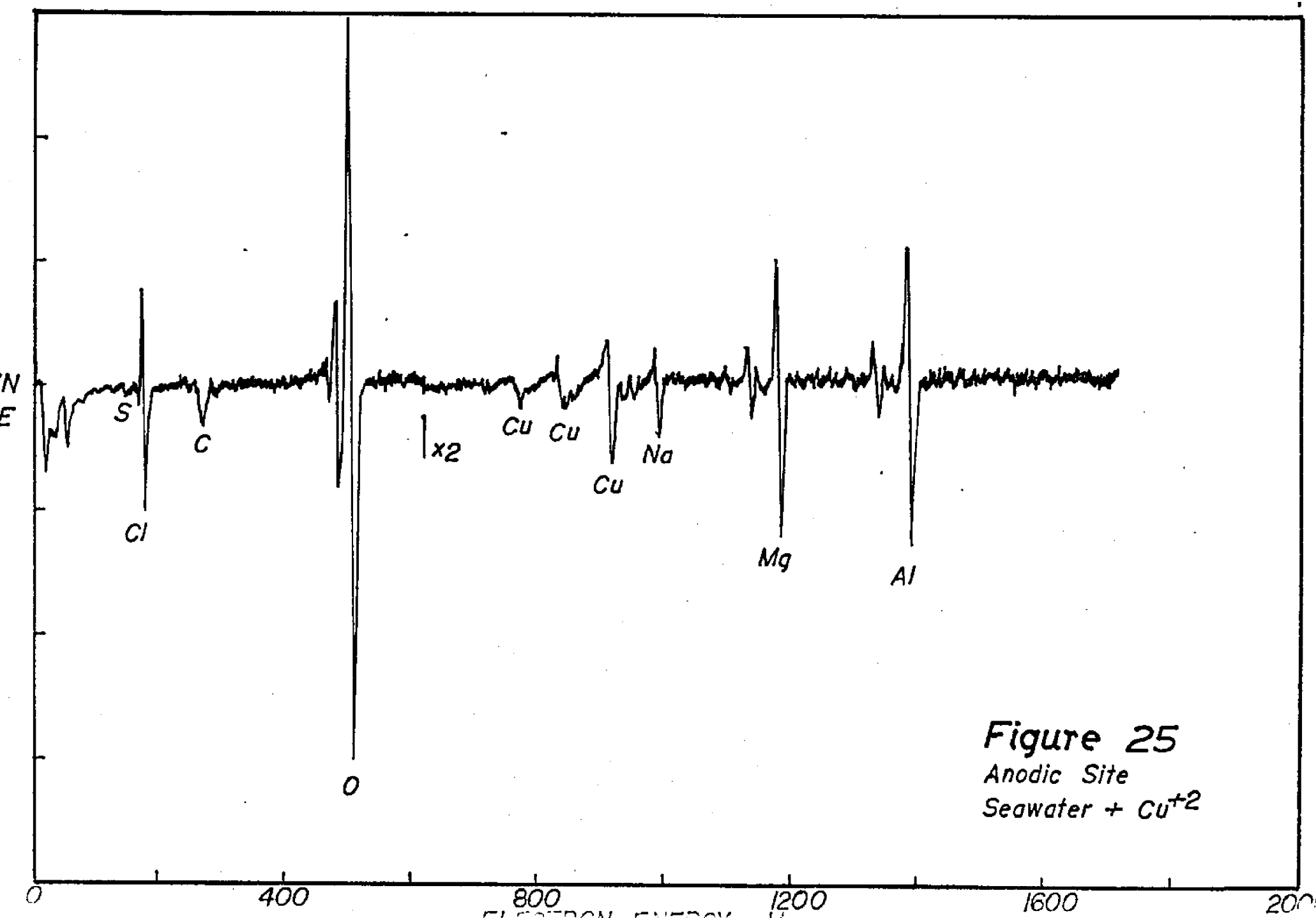

Figure 25
Anodic Site
Seawater + Cu^{+2}

Figure 26
Magnesium Map
Aluminum Surface
Seawater + Cu^{+2}

Complex	Model Fouling Film	Model Sea With Organic	Model Inorganic Seawater
$CuHCO_3$	$0.161X10^{-7}$	$0.471X10^{-7}$	$0.469X10^{-7}$
$CuCO_3^+$	$0.842X10^{-16}$	$0.246X10^{-15}$	$0.245X10^{-15}$
$CuSO_4$	None Detected	$0.587X10^{-17}$	$0.584X10^{-17}$
$CuOH^+$	$0.280X10^{-16}$	$0.818X10^{-17}$	$0.814X10^{-16}$
$Cu(OH)_2$	$0.347X10^{-12}$	$0.102X10^{-11}$	$0.101X10^{-11}$
Cu^{+2}	None Detected	None Detected	$0.325X10^{-9}$
CuX	$0.311X10^{-7}$	$0.909X10^{-10}$	Not Applicable

Figure 27

HALTAFALL Computer Data for Copper Speciation in Seawater

(All Concentrations are Molar)